New Control Strategy for Permanent Magnet Synchronous Generator (PMSG) Wind Turbine

by

Seyed Mehdi MOZAYAN

THESIS PRESENTED TO ÉCOLE DE TECHNOLOGIE SUPÉRIEURE
IN PARTIAL FULFILLMENT FOR THE MASTER'S DEGREE
WITH THESIS IN ELECTRICAL ENGINEERING
M.A.Sc.

MONTREAL, NOVEMBER 30, 2020

ÉCOLE DE TECHNOLOGIE SUPÉRIEURE
UNIVERSITÉ DU QUÉBEC

BOARD OF EXAMINERS

THIS THESIS HAS BEEN EVALUATED

BY THE FOLLOWING BOARD OF EXAMINERS

Mr. Maarouf Saad, Thesis supervisor
Department of Electrical Engineering, École de technologie supérieure

Mr. Handy Fortin-Blanchette, Co-supervisor
Department of Electrical Engineering, École de technologie supérieure

Mrs. Lyne Woodward, President of the board of examiners
Department of Electrical Engineering, École de technologie supérieure

Mr. Ambrish Chandra, Member of the jury
Department of Electrical Engineering, École de technologie supérieure

THIS THESIS WAS PRESENTED AND DEFENDED

IN THE PRESENCE OF A BOARD OF EXAMINERS AND THE PUBLIC

ON "NOVEMBER 04, 2020"

AT ÉCOLE DE TECHNOLOGIE SUPÉRIEURE

ACKNOWLEDGEMENTS

First of all, I would like to express my sincere gratitude to my supervisors, Professor Maarouf Saad and Professor Handy Fortin-Banchette, for their dedicated support during this journey. Thank you for giving me the opportunity to pursue my study at École de technologie supérieure (ÉTS). It was an honor for me to be working with you and I really appreciate your insight throughout my study.

My special thanks go to the committee members, Professor Lyne Woodward and Professor Ambrish Chandra, for going over my thesis and providing valuable comments on this research.

I would like to say a special thank to Professor Mohsen Soltani from Aalborg university. His continued support throughout this project was a motivation for me to take one more step further each time. I hope I can continue to work with him on new challenges for the years to come.

A big thank goes to Hani Vahedi for the valuable discussions we had for our paper published in IEEE Transaction on Industrial Electronics. Thank you for your help and encouragement. You helped me a lot to conduct laboratory experiment for that paper.

I also want to thank my friends at ÉTS. I was so lucky to be surrounded by inspiring students who made our office a great place to focus and study. In particular, I want to thank Soheyl Ziabakhsh, Azeddine Ghodbane, and Jérémy Chambon for their assistance specially when I got stuck in my research.

Last but not least, I would like to dedicate this thesis to my lovely wife, Tahereh Ahmadi Tameh, who always have had my back and I can call her the best friend of mine. I also want to dedicate this project to my newborn angel, Ellin, that brought in meaning to my life.

Last but not least, I would like to dedicate this thesis to my lovely wife, Tahereh Ahmadi Tameh, my parents, and my sisters who always have had my back during this period. I also want to dedicate this project to my newborn angel, Ellin, that brought in meaning to my life.

Nouvelle stratégie de contrôle d'une génératrice synchrone à aimant permanent (PMSG) d'une Éolienne

Seyed Mehdi MOZAYAN

RÉSUMÉ

Grâce à des recherches approfondies dans la communauté des éoliennes, des technologies de pointe ont émergé pour obtenir le bon fonctionnement des éoliennes. Cependant, certaines fonctionnalités doivent être améliorées pour avoir le meilleur système de conversion d'énergie.

Ce mémoire se concentre sur les domaines suivants qui constituent des défis pour les exploitants d'éoliennes:

1. Amélioration de la distorsion harmonique totale (THD) en concevant une stratégie de contrôle avancée.

2. Détection de défaut inter-tours au stade précoce.

Dans la première section de cette thèse, un schéma basé sur le contrôle en mode glissant (SMC) est proposé pour un système de conversion d'éolienne à vitesse variable à entraînement direct (WTCS) équipé d'un générateur synchrone à aimant permanent (PMSG) connecté au réseau. Dans ce travail, un redresseur à diode, un convertisseur de suralimentation, un onduleur à point neutre (NPC) et un filtre en L sont utilisés comme interface entre l'éolienne et le réseau. Cette topologie présente de nombreuses fonctionnalités telles que la simplicité pour les applications d'éoliennes de faible et moyenne puissance. Il est également moins coûteux que les convertisseurs dos à dos à deux niveaux dans les applications de moyenne puissance. L'approche SMC démontre d'excellentes performances dans le contrôle de systèmes non linéaires compliqués tels que WTCS. La stratégie de contrôle proposée modifie la loi d'atteinte (RL) de la technique du mode glissant pour réduire le problème de réticence et pour améliorer la propriété THD par rapport à la loi d'atteinte conventionnelle SMC. L'efficacité de la stratégie de contrôle proposée est explorée par une étude en simulation sur une éolienne de 4 KW, puis vérifiée par des tests expérimentaux pour un montage de 2 KW.

La deuxième section de ce mémoire propose une stratégie de détection et de localisation de défauts basée sur un modèle (FDL) d'une éolienne PMSG montée en surface. L'un des défauts les plus courants dans les éoliennes est le défaut de court-circuit inter-tours (ISC) dans le générateur de WTCS. Pour élaborer le défaut et en observer les conséquences, une éolienne de 120 KW équipée de PMSG est modélisée en injectant le défaut en fonctionnement normal et en régime permanent. L'approche géométrique (GeA) offre de nombreuses fonctionnalités pour FDL dans les applications de contrôle de système non linéaire. Il peut fonctionner comme une fonction intégrée du système de contrôle WTCS dans lequel un défaut ISC est détecté et localisé lorsqu'il se produit dans l'enroulement du stator de PMSG. Le GeA est une technique basée sur un modèle qui fonctionne sur la base des équations gouvernantes du générateur d'éolienne.

L'efficacité du schéma FDL proposé est justifiée par la co-simulation du système de conversion d'énergie éolienne à l'aide des progiciels Maxwell, Simplorer et Matlab.

Mots-clés: Éolienne, générateur synchrone à aimant permanent (PMSG), convertisseur de suralimentation, point neutre bridé (NPC), contrôle en mode glissant (SMC), loi d'atteinte exponentielle améliorée (EERL), contrôle du générateur, contrôle du convertisseur, détection de défaut, système de conversion d'éolienne (WTCS), détection et localisation de défaut (FDL), défaut de court-circuit entre spires (ISC), approche géométrique (GeA)

New Control Strategy for Permanent Magnet Synchronous Generator (PMSG) Wind Turbine

Seyed Mehdi MOZAYAN

ABSTRACT

Due to extensive research in the wind turbine community, advanced technologies have been emerged to obtain the proper operation from wind turbines. However, there are some features needed to be improved to have the best energy conversion system.

This thesis is focusing on following areas which are challenges for wind turbine operators encounter:

1. Improving Total Harmonic Distortion (THD) by designing an advanced control strategy.
2. Inter-turn fault detection at early stage.

In the first section of this thesis, a Sliding Mode Control (SMC) based scheme is proposed for a variable speed, direct-driven Wind Turbine Conversion System (WTCS) equipped with Permanent Magnet Synchronous Generator (PMSG) connected to the grid. In this work, diode rectifier, boost converter, Neutral Point Clamped (NPC) inverter and L filter are used as the interface between the wind turbine and grid. This topology has abundant features such as simplicity for low and medium power wind turbine applications. It is also less costly than back-to-back two-level converters in medium power applications. SMC approach demonstrates great performance in complicated nonlinear systems control such as WTCS. The proposed control strategy modifies Reaching Law (RL) of sliding mode technique to reduce chattering issue and to improve THD property compared to conventional reaching law SMC. The effectiveness of the proposed control strategy is explored by simulation study on a 4 KW wind turbine, and then verified by experimental tests for a 2 KW set-up.

Second section of this thesis proposes a model-based Fault Detection and Localization (FDL) strategy of a surface-mounted PMSG wind turbine. One of the prevalent faults in wind turbines is Inter-turn Short Circuit (ISC) fault in the generator of WTCS. To elaborate the fault and observe the consequences, a 120 KW wind turbine equipped with PMSG is being modeled while injecting the fault during normal and steady state operation. Geometric Approach (GeA) offers plentiful features for FDL in nonlinear system control applications. It can operate as a built-in function of the WTCS control system in which ISC fault is being detected and localized when occurred in the winding of the stator of PMSG. The GeA is a model-based technique that works based upon the governing equations of the generator of wind turbine. The effectiveness of the proposed FDL scheme is justified by co-simulation of wind energy conversion system using Maxwell, Simplorer, and Matlab software packages.

Keywords: Wind Turbine, Permanent Magnet Synchronous Generator (PMSG), Boost Converter, Neutral Point Clamped (NPC), Sliding Mode Control (SMC), Enhanced Exponential Reaching Law (EERL), Generator Control, Converter Control, Fault Detection, Wind Turbine Conversion System (WTCS), Fault Detection and Localization (FDL), Inter-turn Short Circuit (ISC) fault, Geometric Approach (GeA)

TABLE OF CONTENTS

LIST OF TABLES

Page

LIST OF FIGURES

LIST OF ABREVIATIONS

ARL	Adjustable Reaching Law
CANWEA	Canadian Wind Energy Association
CRL	Constant Reaching Law
EERL	Enhanced Exponential Reaching Law
ERL	Exponential Reaching Law
FDL	Fault Detection and Localization
GeA	Geometric Approach
GSC	Grid Side Converter
HAWT	Horizontal-Axis Wind Turbine
IEA	International Energy Agency
IRENA	International Renewable Energy Agency
ISC	Inter-turn Short Circuit
MPPT	Maximum Power Point Tracking
MSC	Machine Side Converter
MTPA	Maximum Torque per Ampere
NRCAN	Natural Resources Canada
PCC	Point of Common Coupling
PI	Proportional Integral
PMSG	Permanent Magnet Synchronous Generator

SMC	Sliding Mode Control
THD	Total Harmonic Distortion
TSR	Tip Speed Ratio
UPF	Unity Power Factor
VAWT	Vertical-Axis Wind Turbine
WTCS	Wind Turbine Conversion System
ZDC	Zero d-Axis Current

INTRODUCTION

Harvesting of clean energy is a key factor for solving environmental issues caused by fossil fuels. There are different sources of renewable energy such as wind, solar PV, hydropower, bioenergy, tidal, etc. The demand for renewable energy has been risen significantly over the course of last decades. The global renewable energy usage has been so far unaffected with respect to the Covid-19 lockdown strategy in different countries, but the installation of new plants is decreased by the situation in 2020. The annual growth of renewable energy generation based on different sources for 2020 is shown in Figure 0.1 (IEA, 2020).

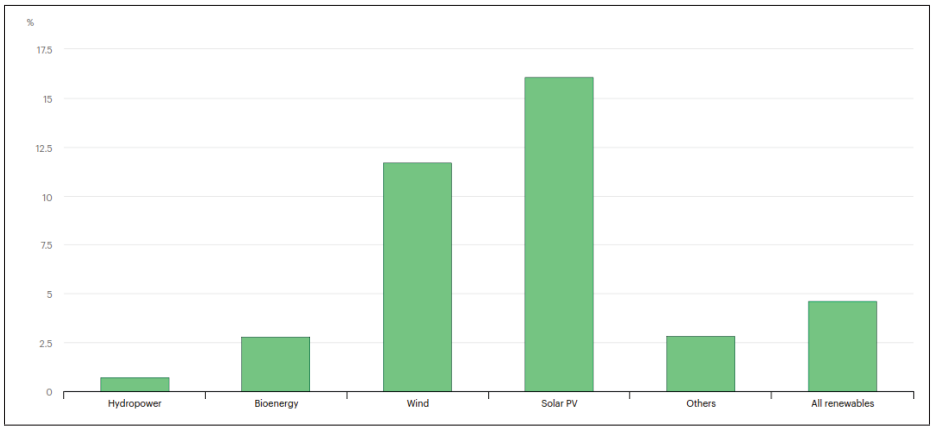

Figure 0.1 Annual growth for renewable energy production of different source for 2020

One of the most promising sources of clean energy is Wind Turbine Conversion System (WTCS) technology. In the past couple of decades, WTCS usage has been raised constantly and their capacity has been increased from small to gigantic wind turbines with a couple of MW power (Blaabjerg, Liserre & Ma, 2012). Nowadays, WTCS technology comes in two categories:

1. **Onshore**: wind turbines installed on land.

2. **Offshore**: wind turbines located in the body of water (e.g. ocean).

Due to ongoing technology disruption, average power of WTCS technology is set to reach 5 MW for onshore and 12 MW for offshore applications in 2025. Recent studies led by researchers show that Wind energy usage will continue to surge in the future. Figure 0.2 and Figure 0.3 depict annual onshore and offshore wind facility additions until 2050 respectively (IRENA, 2019).

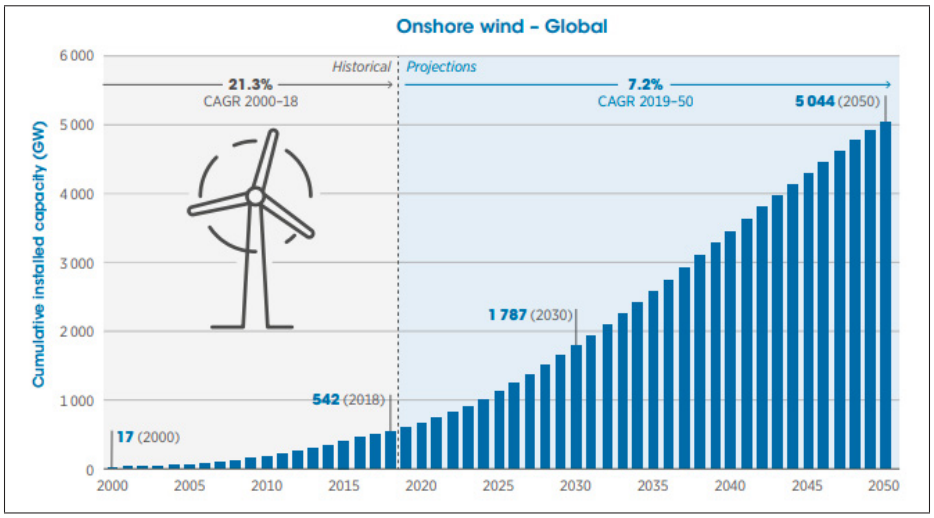

Figure 0.2 Annual onshore wind facility addition projection in the world until 2050

Based on Figure 0.2 and Figure 0.3, annual onshore and offshore wind facility additions will be approximately 10 fold in 2050 compared to 2018. Table 0.1 provides wind generation capacity of top 10 countries in the world in 2018 (NRCAN, 2020).

Geographical situation of Canada makes it suitable to harvest huge amounts of energy from wind, therefore wind power is captured all across the country. Figure 0.4 shows the installed wind power capacity in Canada as of December 2019 which 13,413 MW with 301 wind farms in the service from coast to coast. This amount of power generated by wind can provide electricity to roughly 3.4 million homes. In 2019, Ontario and Quebec produced the most wind power with 5,436 MW and 3,882 MW, respectively (CANWEA, 2020). Based on the information from

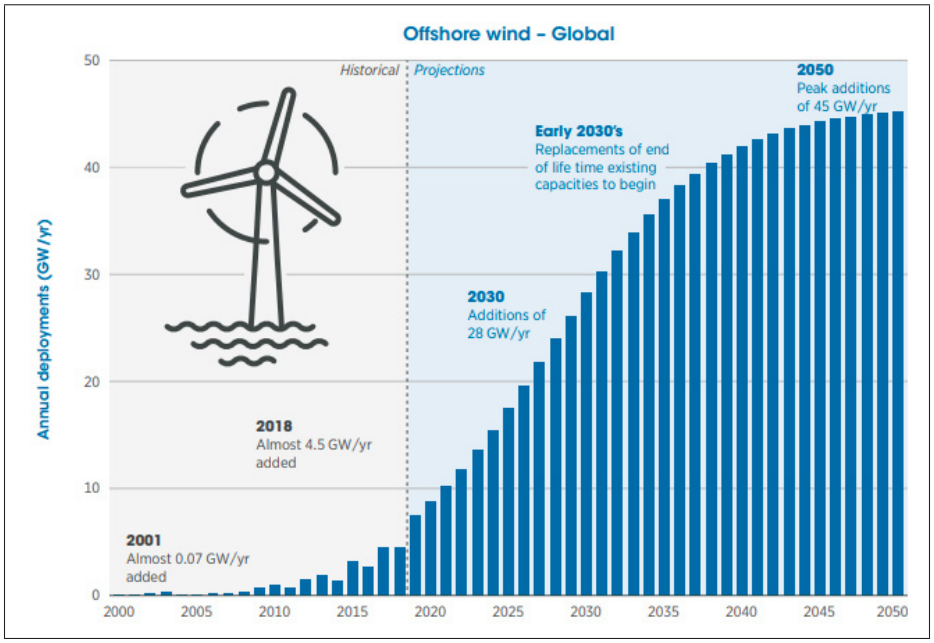

Figure 0.3 Annual offshore wind facility addition projection in the world until 2050

Table 0.1 World capacity of wind power in 2018 – 591,549 MW

Rank	Country	Percentage
1	China	36%
2	United States	16%
3	Germany	10%
4	India	6%
5	Spain	4%
6	United Kingdom	4%
7	France	3%
8	Brazil	2%
9	Canada	2%
10	Italy	2%

Natural Resources Canada, wind energy accounts for 4% of the total power generated in 2018 in Canada (NRCAN, 2020).

Wind turbines are designed to operate in fixed-speed or variable-speed modes. Fixed-speed wind turbines, as their name indicate, operate in the constant speed and have simple structures which

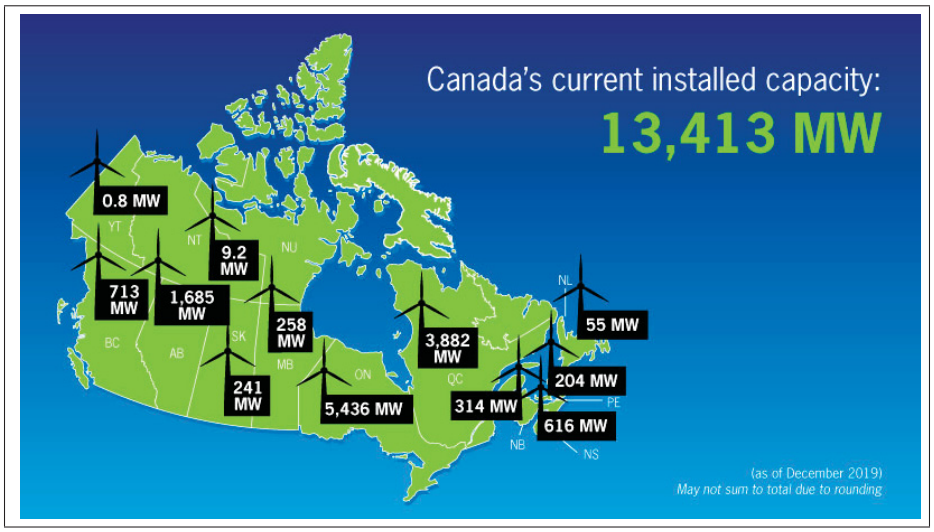

Figure 0.4 Canada's current installed wind turbine capacity

are suitable for certain situations. On the other hand, rotational speed of variable-speed wind turbines is adjusted related to the wind speed. Therefore, the efficiency of the variable-speed wind turbines is higher than the fixed-speed ones (Xu, Blaabjerg, Chen & Zhu, 2018). As seen in Figure 0.5, different generator technologies are used in WTCS.

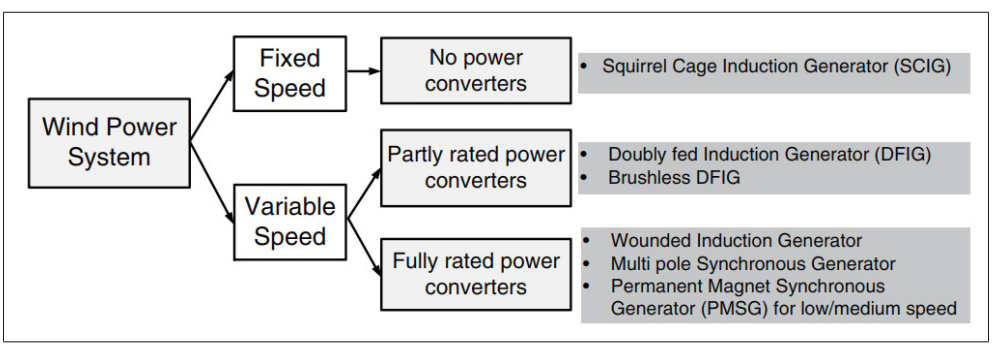

Figure 0.5 Generator technologies used in WTCS

According to the appearance of the wind turbines, they are basically classified as: Horizontal-Axis Wind Turbine (HAWT) and Vertical-Axis Wind Turbines (VAWT). Rotor shafts in HAWT and VAWT are in parallel and perpendicular to the ground, respectively. Generally, the location

of the generator and gearbox in HAWT is at the top of the tower, while in VAWT it is at the bottom of the tower. Figure 0.6 demonstrates horizontal and vertical axis types of WTCS.

Figure 0.6 HAWT (left) and VAWT (right)

CHAPTER 1

LITERATURE REVIEW

The presence of wind turbine power plants is on the rise in different regions in the world. It is expected that WTCS is going to have more impact in the electrical energy generation by integrating more wind farms to the power grid. Therefore; wind turbine advanced control is an indispensable aspect of integration to the power system to achieve smooth connection specially for the large scale wind turbines. The goal of the WTCS control is to optimize the operation such that WTCS can handle the unpredictable characteristics of wind resources.

Permanent magnet synchronous generators (PMSGs) have gained more attraction in the wind turbine community compared to other types of generators due to (Polinder, van der Pijl, de Vilder & Tavner, 2006):

1. Light weight and volume.
2. Elimination of dc excitation current.
3. High efficiency and reliability.
4. High torque to volume ratio.

Hence, regarding the generator type of the WTCS, the focus of this thesis goes towards the PMSG technology. As the operation of WTCS is dependent on the wind speed, advanced control strategy has to be designed for such a complex system to obtain optimum operation of wind turbines. Moreover wind turbines are mostly working in severe weather conditions, so they are prone to experience different faults. Fault detection scheme is gained popularity in the wind turbine industry specially for offshore applications to decrease the amount of time the wind turbine is not in service (downtime).

1.1 Control of PMSG Wind Turbines

In PMSG based WTCS, the generator is directly connected to the electrical network through a power converter. To connect the PMSG to the electrical network, full scale power electronic system is required to regulate all the energy from WTCS to power network. As the power converter needs to have the capability to transfer all the power generated by WTCS, the commonly used two level back to back converter is not a suitable topology for high power PMSG wind turbine due to high switching loss and cabling design challenges. Various power electronic converter topologies have been proposed to engage in wind turbine applications. Among these topologies, Neutral Point Clamped (NPC) converters are gaining prominence to play an interface role in grid-tied WTCS applications because it outputs more voltage level while having less switch stress (Vahedi & Al-Haddad, 2016; Vahedi, Labbé & Al-Haddad, 2016). These advantages of NPC converter make it promising to transfer the electrical energy at low to medium voltage with lower current, less paralleled devices, and reduced size of filter in comparison with two-level converter (Blaabjerg & Ma, 2013; Sharifzadeh, Vahedi, Portillo, Khenar, Sheikholeslami, Franquelo & Al-Haddad, 2016). The integration of megawatt range wind turbines to the power grid is bringing new problems associated with voltage and frequency control of Point of Common Coupling (PCC).

Most studies in the field of WTCS are dedicated to the development of appropriate control techniques to increase its ability to supply and regulate active and reactive power in both grid connected and islanding modes (Delfino, Pampararo, Procopio & Rossi, 2012). Several control approaches have been applied for PMSG based WTCS control to reduce generator currents, to extract maximum power from wind turbines, to keep DC link voltage constant, to control the reactive power injected to the grid, and to decrease current harmonics at PCC. These control strategies of PMSG wind turbines can be generally arranged into two categories (Zhong, Ma, Ming & Konstantopoulos, 2015). In the first category, Maximum Power Point Tracking (MPPT) is achieved by Machine Side Converter (MSC) control, whereas the DC link voltage is governed by Grid Side Converter (GSC) control (Li, Haskew, Swatloski & Gathings, 2012; Muyeen & Al-Durra, 2013; Rajaei, Mohamadian & Yazdian Varjani, 2013). In the second one,

GSC adjusts the active power extraction from wind turbine, and the DC link voltage control is obtained by MSC control (Yuan, Wang, Boroyevich, Li & Burgos, 2009). In both cases, vector control is applied to achieve control objectives.

Different control schemes have been developed to achieve the control objectives of PMSG based WTCS operation. Three prevalent methods being used to achieve the control goals are: Zero d-Axis Current (ZDC) control, Maximum Torque per Ampere (MTPA) control, and Unity Power Factor (UPF) control (Wu, Lang, Zargari & Kouro, 2011).

Researchers have adopted different linear control schemes to control grid-connected inverter (Kuschke & Strunz, 2014; Trilla, Bianchi & Gomis-Bellmunt, 2014). However, these solutions have main disadvantages such as: incapability to track sinusoidal trajectory references and poor capability to reject system disturbance. Generally, linear approaches (PI control strategy) have the ability to meet some of the operation necessities (Hao, Yang, Liu, Huang & Chen, 2013). Several studies have been conducted focusing on nonlinear techniques to control grid-tied PMSG (Kim, Jeung, Lee & Kim, 2012; Rigatos, Siano & Zervos, 2014). These methods are sensitive to modeling errors, difficult to implement, and require the exact PMSG parameters (Kim, Song & Lee, 2015; Zhang, Gadsden & Habibi, 2013). On the other hand, Sliding Mode Control (SMC) method, as one of the control approaches in both linear and nonlinear systems, has gained a lot of attention due to its robustness, order reduction, insensitivity to parameter variations, finite-time convergence, disturbance rejection, good dynamic behavior, and simple implementation (Haq, Khan, Khan, Akmeliawati, Nisar & Khan, 2020; Sarsembayev, Suleimenov, Mirzagalikova & Do, 2020; Sebaaly, Vahedi, Kanaan, Moubayed & Al-Haddad, 2014; Shtessel, Edwards, Fridman & Levant, 2014).

The main drawback of SMC is the chattering phenomenon because of discontinuous function in SMC. Many approaches have been proposed to eliminate or attenuate chattering issue which is undesirable in some applications (Fallaha, Saad, Kanaan & Al-Haddad, 2011; Hao *et al.*, 2013; Valenciaga & Puleston, 2008). An interesting method to reduce chattering phenomenon is to use Adjustable Reaching Law (ARL) instead of having a Constant Reaching Law (CRL)

gain in SMC (Fallaha *et al.*, 2011; Gao & Hung, 1993). A kind of ARL based on applying an exponential term in the reaching law was proposed in (Fallaha *et al.*, 2011) which improves chattering reduction aspect of the controller but it can be further improved in some aspects to be applied in power electronics applications such as Total Harmonic Distortion (THD) improvement of grid current at PCC.

The proposed ARL sliding mode technique in Chapter 4 of this thesis performs the controller gain correction based on the discrepancy between the actual and desired system states (error signal). When the error value is high, the gain is increased in order to force the system state to move toward the desired state as fast as possible. When the error signal becomes small, the applied gain is going to decrease in a way that once the gain tends to zero, the error inclines to zero. It is worth noting that the ARL approaches suggested in the literature do not amend the gain in a wise manner in the wide range of error values from zero- to high-error quantities. Therefore, the proposed approach is more pragmatic than the methods proposed in (Fallaha *et al.*, 2011; Gao & Hung, 1993).

1.2 Fault Detection of PMSG Wind Turbines

Safety concerns of industrial systems have forced researchers to investigate extensively fault detection algorithms and their applications to complex systems over the past two decades. As wind turbines are mostly operating in harsh environment, they are subject to different faults which are classified based on the failure rates and turbine downtime. Gearbox and generator of the wind turbines have the longest downtime in WTCS systems, respectively (Ribrant & Bertling, 2007). Therefore, the manufactures are focusing more on the gearless Permanent Magnet Synchronous Generator (PMSG) wind turbines, especially in offshore applications. It is also important to note that the generators failure rate in WTCS varies between 0.04 and 0.2 failures per year which is higher than the average failure rate of industrial machines which is about 0.04 failures per year (Tavner, 2008). The wind turbines connected to the power system are subject to impulse voltages, generated by lightning strikes, faults in the power system, and switching operations. Impulse voltages might lead to winding flash-over if not detected at

the incipient stage, it will deteriorate the winding insulation causing a forced shutdown of the turbine. A large current will be flowing in the short-circuited turns of PMSG while the generator output currents will be small. This phenomenon is happened due to the small ratio between the short-circuited turns and complete winding. Studies show that the stator winding faults constitute the largest portion of the electrical faults. Machine winding faults usually start as an undetected insulation failure between two adjacent turns, and then develop into the phase to ground or phase to phase short circuit faults (Ebrahimi, Faiz & Roshtkhari, 2009; Vaseghi, Takorabet, Nahid-Mobarakeh & Meibody-Tabar, 2011). Therefore, appropriate action should be taken to protect the PMSG with the stator short-circuited winding.

Several approaches have been proposed for fault detection in permanent magnet machines such as signal-based, knowledge-based, and model-based approaches (Beddek, Merabet, Kesraoui, Tanvir & Beguenane, 2017; Da, Shi & Krishnamurthy, 2013; Nyanteh, Edrington, Srivastava & Cartes, 2013; Tan, Zhang & Zhou, 2020). However, model-based approach is often considered as the preferred method for fault detection if an accurate mathematical model of the system can be constructed (Aubert, Regnier, Caux & Alejo, 2015; Ghodbane, Saad, Hobeika, Boland & Thibeault, 2016; Sarikhani & Mohammed, 2013). Most suggested fault detection methods have following drawbacks:

1. They are complicated.
2. They are not robust to parameter variations.

Model-based fault detection schemes are working relying on residual generation to be able to recognize the fault in the system (Isermann, 2006). Figure 1.1 depicts the overview of residual generation for Fault Detection and Localization (FDL). One of the model-based approaches for FDL that has gained attraction for complex plants is Geometric Approach (GeA).

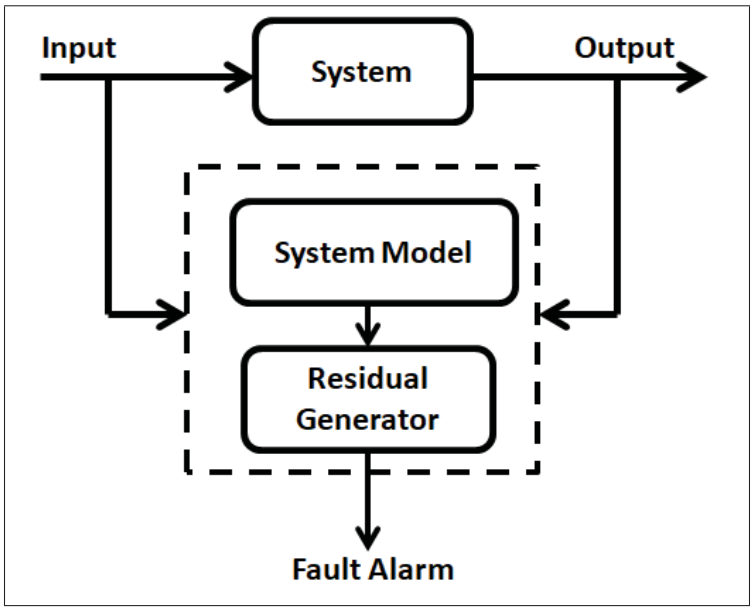

Figure 1.1 The general concept of residual generation for fault detection

1.3 Motivations and Objectives

The amount of energy that can be captured by wind turbines is limited, hence it becomes vital to come up with an algorithm to maximize the converted energy. However, traditional control systems such as the proportional integral (PI) controller which is commonly used in different industries has numerous problems such as sensitivity to parameter variations for the control of such a nonlinear system. Therefore; designing an advanced controller is a necessity for WTCS control.

Wind turbines are also costly devices in the power grid, so wind farm operators would like to keep wind turbines in service in the optimal working situation, and manage their assets such that faults specially inter-turn short circuit ones are detected as soon as possible. The main objectives of this thesis are as follows:

1. To develop an advanced control system to capture most of the energy available in the wind and provide a high quality generated power at the point of connection to the power grid while meeting the requirement imposed by the power system standard.

2. To design a controller to detect an incipient short circuit fault before propagation in the whole system which results in the wind turbine shut down.

1.4 Thesis Outline

This thesis is structured as follows. Dynamic model of the wind turbine is explained in Chapter 2. In Chapter 3, modeling of PMSG wind turbine is described . In Chapter 4, we propose an SMC-based controller, called enhanced exponential reaching law (EERL) sliding mode approach which can meet the requirements in power applications. The contributions of this method are three folds: first, EERL reduces the reaching time of system trajectory to the equilibrium point even the initial condition of the system parameters are far from the sliding surface. Second, EERL has the capability to further mitigate chattering issue of sliding mode approach with respect to the conventional SMC. Then, EERL improves current THD of the grid-connected inverter which is vital for distributed generation integration into the power grid. In this study, power control of PMSG is carried out by boost converter and UPF method is applied for NPC inverter control. Numerical simulation and experimental results of the proposed SMC-based controller are reported in Chapter 5. In Chapter 6 of this thesis, we will be applying GeA for detecting the fault and its location in the winding of the wind turbine generator. In the GeA, a projector is defined in order to have the state space model of the WTCS generator decomposed in two different parts such that one of them is tangent and the other one is transverse to the unknown input of the system. In fact, the unknown input is the emerging fault in the generator winding. The GeA provides a precious tool to detect the fault occurred in linear and nonlinear dynamic systems with residual sets. The strength of the GeA is in its ability to detect incipient Inter-turn Short Circuit (ISC) fault before it is expanded to a catastrophic situation. Therefore, the contributions of this method are three folds. First, the ISC fault of the generator is modeled in the Maxwell software. Second, GeA detects the ISC fault in the generator in a reasonable

time frame before leading to system failure. Third, the GeA provides the location (phase a, b, or c) of the early ISC fault.

CHAPTER 2

DYNAMIC MODEL OF WIND TURBINE CONVERSION SYSTEM

The aerodynamic torque made by forces acting on the blades is transferred to the generator via the drive train. Then the generator converts the mechanical energy into electrical energy. This energy is injected to the grid through power electronic devices to the grid to meet the required objectives. There are different power electronic topologies for integrating the wind turbine to the power system.

The theoretically available power in the wind can be stated as:

$$P_{available} = \frac{1}{2}\rho A v_w^3 \tag{2.1}$$

where ρ, v and A are the air density (kg/m^3), the wind speed (m/s) and the swept area of rotor blades (m^2), respectively. Due to physical limits (e.g., Betz limit), not all of the power can be captured by a WECS, so wind turbine blades only transfer portion of the wind kinetic energy. The absorbed mechanical power by rotor is given by the following expression

$$P_t = \frac{1}{2}\pi\rho R^2 v_w^3 C_p(\lambda, \beta) \tag{2.2}$$

where C_p is power coefficient. In WTCS aerodynamics, there are two main variables that make C_p change: blade pitch angle β and tip speed ratio (TSR) of the blade $\lambda = R\omega_{rm}/v_\omega$ in which R and ω_{rm} are the rotor plane radius and the angular velocity of the rotor, respectively.

In the literature, models with different levels of complexity are available for the drive train subsystem. The available drive train models of the WTCS are six-mass model, three-mass model, two-mass model and one-mass (lumped) model (Muyeen, Tamura & Murata, 2009).

The generation capacity of a wind turbine system determines how much power can be captured from the wind. It is usually specified by a curve based on the generator output power versus actual wind speed which is called WTCS power curve. The wind speed operational range in WTCS is between the cut-in ($v_{\omega-min}$) and cut-out ($v_{\omega-max}$) wind speeds. In the wind speeds lower than $v_{\omega-min}$ and higher than $v_{\omega-max}$ (regions I,IV), the wind turbine system is shut down (or may spin freely in region I). At wind speeds below the $v_{\omega-min}$, the available energy is not enough for power production. As the wind speed increases above the $v_{\omega-max}$, the turbine is stopped to avoid turbine from damage. The WTCS operation can be described in four different regions based on the wind speed. At wind speeds between $v_{\omega-min}$ and nominal speed (region II), the available wind power would be lower than generator rated power. So, the generation goal in this operation region is to capture maximum power. Hence, the extracted power in this region is calculated by:

$$P_t = \frac{1}{2}\pi\rho R^2 v_w^3 C_{p-max} \tag{2.3}$$

In the wind speed higher than rated wind speed value and lower than $v_{\omega-max}$ (region III), the WECS power curve remains constant at rated power. Therefore the wind turbine must operate with power coefficients lower than C_{p-max}. Figure 2.1 demonstrates power curve of a typical wind turbine in which working regions are explicitly shown.

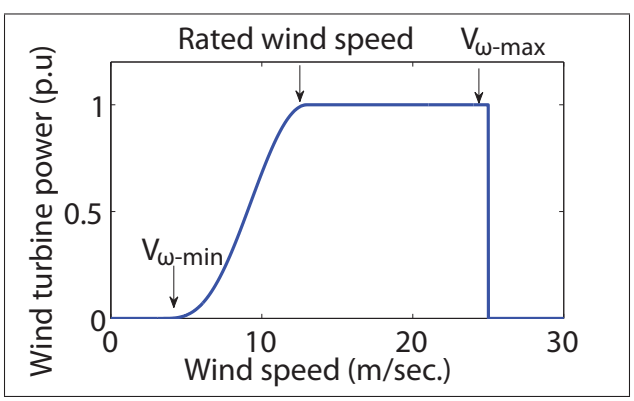

Figure 2.1 Typical power curve of wind turbine systems

CHAPTER 3

PERMANENT MAGNET SYNCHRONOUS GENERATOR MODELING

To explore the behavior of the wind turbine, different parts of the WTCS must be modeled. Therefore, the objective of this chapter is to model permanent magnet synchronous generator which is used in Chapters 4 and 6. Other components are modeled in following chapters if it is required.

3.1 PMSG Model in dq Reference Frame

Dynamic model of the surface mounted PMSG in dq rotor reference frame is very common in the literature such as in (Krause, Wasynczuk, Sudhoff & Pekarek, 2013) and can be expressed by:

$$\frac{di_{ds}}{dt} = -\frac{R_s}{L_s} i_{ds} + \omega_{re} i_{qs} + \frac{1}{L_s} v_{ds} \tag{3.1}$$

$$\frac{di_{qs}}{dt} = -\frac{R_s}{L_s} i_{qs} - \omega_{re} i_{ds} - \frac{\lambda_f}{L_s} \omega_{re} + \frac{1}{L_s} v_{qs} \tag{3.2}$$

$$\frac{d\omega_{rm}}{dt} = \frac{1}{J}(T_t - T_e) \tag{3.3}$$

The provided equations will be useful when designing advanced control method for WTCS in Chapter 4.

3.2 PMSG Model in abc Reference Frame

For the sake of model-based fault detection system, governing equations of PMSG are presented here. As we would like to detect and localize the fault for specific phase, we are not going to employ the PMSG model in the dq reference frame because it will need more calculation and analysis to find the fault location after the ISC fault is detected in the electrical machine

(Lu, of Manchester, University of Manchester. School of Mechanical & Engineering, 2011). Therefore, abc reference frame is chosen to elaborate the fault detection scheme on. The equation of a healthy PMSG is given as:

$$[v_s] = [R_s][i_s] + [L_s]\frac{d[i_s]}{dt} + \frac{d}{dt}[\Psi_r] \tag{3.4}$$

where $[v_s]$, $[i_s]$, $[R_s]$, $[L_s]$, and $[\Psi_r]$ are voltage, current, resistance, inductance, and permanent magnet flux linkage matrices respectively. Subscripts s and r represent stator and rotor of the generator. The mentioned matrices are written as:

$$[v_s] = \begin{bmatrix} v_{sa} \\ v_{sb} \\ v_{sc} \end{bmatrix} \tag{3.5}$$

$$[i_s] = \begin{bmatrix} i_{sa} \\ i_{sb} \\ i_{sc} \end{bmatrix} \tag{3.6}$$

$$[\Psi_r] = \begin{bmatrix} \Psi_m sin\theta_{re} \\ \Psi_m sin(\theta_{re} - \frac{2\pi}{3}) \\ \Psi_m sin(\theta_{re} + \frac{2\pi}{3}) \end{bmatrix} \tag{3.7}$$

$$[R_s] = \begin{bmatrix} R_a & 0 & 0 \\ 0 & R_b & 0 \\ 0 & 0 & R_c \end{bmatrix} \tag{3.8}$$

$$[L_s] = \begin{bmatrix} L_a & M_{ab} & M_{ac} \\ M_{ba} & L_b & M_{bc} \\ M_{ca} & M_{cb} & L_c \end{bmatrix} \tag{3.9}$$

where Ψ_m and θ_{re} are the maximum flux linkage established by rotor permanent magnet and electrical rotor position. In the inductance matrix, L and M are self inductance and mutual inductance, respectively. Note that due to identical magnetic path in the surface mounted PMSG, position of the rotor does not have any implication on the inductance matrix of the generator.

Mechanical equation of the wind turbine takes the following form:

$$\frac{d}{dt}\omega_{rm} = \frac{1}{J}\left(T_t - T_e - B\omega_{rm}\right) \tag{3.10}$$

where J, T_t, T_e, B, and ω_{rm} are inertia, turbine torque, electromagnetic torque, viscous damping coefficient, and rotor mechanical speed, respectively. It is worth mentioning that mechanical and electrical parameters (ω and θ) are related as a function of generator pole numbers. Hence, the relationship between the electrical and mechanical speed is:

$$\omega_{re} = \frac{n_p}{2}\omega_{rm} \tag{3.11}$$

where ω_{re} and n_p are the electrical speed of the rotor and number of poles of the generator. Therefore, the state, input, and output vectors are as follows:

$$\begin{cases} x = \begin{bmatrix} i_{sa} & i_{sb} & i_{sc} & \theta_{re} & \omega_{re} \end{bmatrix}^T \\ u = \begin{bmatrix} v_{sa} & v_{sb} & v_{sc} & T_t \end{bmatrix}^T \\ y = \begin{bmatrix} i_{sa} & i_{sb} & i_{sc} \end{bmatrix}^T \end{cases} \tag{3.12}$$

The provided equations in this section will help us develop fault detection strategy in Chapter 6.

CHAPTER 4

SLIDING MODE CONTROL OF PMSG WIND TURBINES

The aim of this chapter is to design an advanced control system by using the Sliding Mode Control (SMC) approach for PMSG equipped wind turbine. To develop the controller, following devices are used as the interface between the wind turbine and power grid: diode rectifier, boost converter, neutral point clamped inverter, and L filter. This topology has abundant features such as simplicity for low- and medium power wind turbine applications. It is also less costly than back-to-back two-level converters in medium-power applications.

4.1 SMC Theory Based On Modified Reaching Law

Mathematical model of real plants are always imprecise. This mismatch can be generated due to parametric uncertainties and unmodeled dynamics. Thus, a control system is needed to be robust to these inaccuracies to have the strength of keeping the system performance stable. SMC is a powerful robust control method for uncertain systems that has been widely researched in both theoretical and industrial application aspects. The general concept of SMC theory is explained in (Slotine & Li, 1991). As a motivation to overcome aforementioned limitations, a new reaching law will be presented and formulated in this chapter. Intuitively, SMC methodology replaces n^{th}-order system by a first-order system which can be controlled easily by choosing a well-mannered function of the tracking error called sliding surface or sliding manifold. It moves the system trajectory from its initial point to the sliding manifold in finite time, and then constrains the variables such that to lie within a vicinity of the sliding surface by a control law. For illustration purposes of SMC theory, a second-order nonlinear system with following state equation is considered:

$$\ddot{x} = f(x, \dot{x}) + g(x, \dot{x})u \tag{4.1}$$

where x and u are state and input vectors; and f and g are bounded nonlinear matrix functions of the system states. It is supposed that function g is continuous and invertible. The control aim is to get the state vector to track the desired state vector in the presence of disturbances and uncertainties. Let $\widetilde{x} = x - x_d$ be the trajectory error in state vector x, where x_d is desired state vector. Conventionally, time-varying sliding surface for a nth order system is chosen as:

$$S(t) = (\frac{d}{dt} + \Lambda)^{n-1}(x - x_d) \tag{4.2}$$

where Λ is a strictly positive number. For second order systems, one can define following surface

$$S(t) = \Lambda\widetilde{x} + \dot{\widetilde{x}} \tag{4.3}$$

Therefore, the problem of tracking the desired vector is equivalent to keeping S at zero all the times. In fact, there are two different modes in SMC methodology. In reaching stage, tracking error vector $\widetilde{x}$ is reached to the sliding surface $S = 0$ in a finite time. Since sliding surface is an invariant set, system trajectory slides and remains on $S = 0$ in sliding stage. It is worth mentioning that S can be selected as $x - x_d$ for first order systems.

The problem of keeping the error vector on the sliding surface can be obtained by defining the control law u such that:

$$\frac{1}{2}\frac{d}{dt}S^2 \leq -\eta\,|S| \tag{4.4}$$

where η is a strictly positive constant. Satisfying above condition keeps the system trajectories remaining on the sliding surface. Sliding condition (Equation 4.4) can be expressed as:

$$S\dot{S} \leq 0 \tag{4.5}$$

Integrating Equation 4.4, results in:

$$t_{reach} \leq |S(t=0)| / \eta \tag{4.6}$$

where t_{reach}, reaching time, is the required time for $\widetilde{x}$ to reach the sliding surface. With the purpose of satisfying expression Equation 4.5, $\dot{S}$ is generally taken as:

$$\dot{S} = -K sign(S) \tag{4.7}$$

where $sign$ is the sign function and K is also a positive constant. Choosing K large enough guarantees sliding condition in constant rate reaching law SMC. To satisfy sliding condition despite uncertainty in the system, a discontinuous term can be added to control input (Slotine & Li, 1991). Accordingly our control input takes the form:

$$u = u_{con} + u_{discon} \tag{4.8}$$

Therefore, it is as follows:

$$u = g^{-1}(-f + \ddot{x}_d - \Lambda\widetilde{x} - K sign(S)) \tag{4.9}$$

It is obvious that control law is composed of two terms. Discontinuous term which is applied due to imprecision of system modeling and disturbances, leads to an undesired phenomenon called chattering. Chattering might stimulate ignored high frequency dynamics of the system model. Choosing appropriate value of K would be a trade-off between reaching time and level of chattering. This method is called constant reaching law (CRL) sliding mode approach. Several works are done to attenuate or eliminate the chattering issue by modifying reaching law. In

(Gao & Hung, 1993), they proposed constant-proportional rate reaching law and power rate reaching law. Constant-proportional rate reaching law has the form:

$$\dot{S} = -\Lambda S - K sign(S) \tag{4.10}$$

Definite integration of Equation 4.10 between zero and t_{reach} leads to:

$$\int_{S(t=0)=S_0}^{S(t_{reach})} \frac{dS}{\Lambda S + K sign(S)} = \int_0^{t_{reach}} -dt \tag{4.11}$$

Note that $S(t_{reach}) = 0$. For $S \geq 0$, reaching time is:

$$t_{reach} = \frac{1}{\Lambda} ln \frac{\Lambda S_0 + K}{K} \tag{4.12}$$

If $S \leq 0$, it yields:

$$t_{reach} = \frac{1}{\Lambda} ln \frac{-\Lambda S_0 + K}{K} \tag{4.13}$$

Therefore, one can simply express the reaching time in all conditions as:

$$t_{reach} = \frac{1}{\Lambda} ln \frac{\Lambda |S_0| + K}{K} \tag{4.14}$$

The main disadvantage of Equation 4.10 is that reaching law is not adjustable. Power rate reaching scheme is as

$$\dot{S} = -K|S|^{\gamma_x} sign(S) \tag{4.15}$$

where $0 < \gamma_x < 1$ and $K > 0$. By applying the same procedure as explained before, the reaching time is as:

$$t_{reach} = \frac{1}{(1-\gamma_x)K}|S_0|^{(1-\gamma_x)} \tag{4.16}$$

The demerit feature of Equation 4.15 is the reduction of its robustness due to the rapid lessening of the exponential term $|S|^{\gamma_x}$. In (Fallaha *et al.*, 2011), an additional term is introduced to reduce chattering problem in robot applications by defining following function to handle reaching law:

$$\dot{S} = -\frac{K}{D(S)} sign(S) \tag{4.17}$$

where

$$D(S) = \alpha + (1-\alpha)e^{-\beta_x|S|} \tag{4.18}$$

In Equation 4.18, $0 < \alpha < 1$ and $\beta_x > 0$. This method is called Exponential Reaching Law (ERL) approach. The reaching time for ERL is obtained as:

$$t_{reach} = \frac{1}{K}(\alpha|S_0| + \frac{(1-\alpha)}{\beta_x}[1 - e^{-\beta_x|S_0|}]) \tag{4.19}$$

This method brings a lot of advantages such as gain adaptation based on the position of S_0 regarding the sliding surface, smaller reaching time and chattering reduction but shows a higher THD than our proposed method which might cause problem in power electronics application.

To solve above mentioned issues, an EERL is applied which is a combination of different concepts in (Fallaha *et al.*, 2011; Gao & Hung, 1993) as well as applying new structure for

managing the reaching law in both reaching and sliding stages. Our proposed EERL is as follows:

$$\dot{S} = -\Lambda S - \frac{K}{D(S)}|S|^{\gamma_x} sign(S) \tag{4.20}$$

It is obvious if α tends to 1, proposed EERL is converted to power rate reaching law. Note that $D(S)$ is strictly positive at all time, therefore it does not have any impact on the SMC approach stability. In the proposed EERL, if the absolute value of S raises, D(S) goes towards α, then coefficient of sign function would be $K|S|^{\gamma_x}/\alpha$. In contrast, when absolute value of S reduces, it tends to $K|S|^{\gamma_x}$. This phenomenon makes the controller gain to be modified between $K|S|^{\gamma_x}$ and $K|S|^{\gamma_x}/\alpha$; therefore, it adjusts the reaching time to get to the sliding surface. In other words, EERL approach specifies faster reaching speed or smaller reaching time with respect to the constant rate reaching law SMC considering similar gain K. In addition, existence of Λ and γ_x along with $D(S)$ simultaneously in the controller will augment the characteristics of the controller while eliminating the disadvantages of each approach.

Figure 4.1 illustrates the effect of the coefficient of sign function using the methods explained before. From Figure 4.1, one can see that when $|S|$ is small, coefficient of sign function in methods ERL and EERL are approximately the same. On the contrary, when $|S|$ increases, coefficient in EERL concept becomes bigger than coefficient in ERL approach. It signifies that attraction of system trajectory to the sliding surface in EERL in high $|S|$ is faster than ERL. When the system state comes closer to the sliding surface, coefficients of both ERL and EERL methods gently diminish to mitigate the chattering problem. This figure explicitly exhibits that the gain of EERL decrease a lot when $|S|$ is extremely small, while in ERL the gain will approach K when $|S|$ is even near zero. Hereupon, the gain of EERL is altered elaborately to span the whole range of error vector x, no matter how big or small the error is. Consequently, EERL method manipulates the system states more suitable than ERL whenever $|S|$ is very high or very small. Figure 4.1 also indicates that sign coefficient associated with power rate approach

would be always near zero, when γ is chosen small. Moreover, constant rate approach provides constant coefficient all the time.

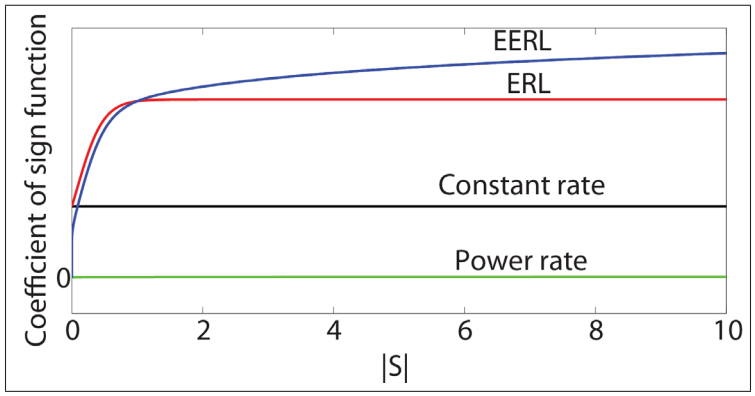

Figure 4.1 Sign coefficient comparison based on different SMC methods

4.2 Dynamic Model of the PMSG Based Wind Turbine

This section briefly explains elements of the system and provides their governing equations. Figure 4.2 demonstrates the overview of grid connected PMSG-based WTCS. The aerodynamic torque made by forces acting on the blades is transferred to PMSG via the drive train. Then, PMSG converts the mechanical energy into electrical energy. This energy is injected to the grid through diode rectifier, boost converter, NPC inverter, and L filter to meet the required objectives. This topology is used in both low- and medium-voltage applications (Blaabjerg *et al.*, 2012; Orlando, Liserre, Mastromauro & Dell'Aquila, 2013; Yaramasu & Wu, 2014; Yaramasu, Wu, Alepuz & Kouro, 2014). The advantages of this scheme are: simple control and system cost reduction (Trilla *et al.*, 2014).

To investigate wind turbine dynamic behavior, it is necessary to model the components of the WTCS. Dynamic model of the mechanical part and the surface mounted PMSG in dq rotor reference frame were explained in Introduction and Chapter 3, respectively.

To model the boost converter, following equations are used:

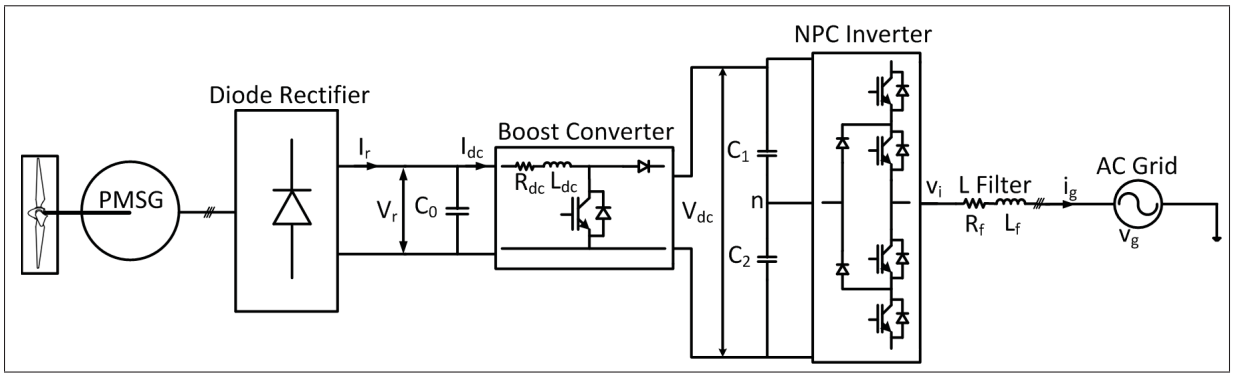

Figure 4.2 General overview of grid connected PMSG

$$\frac{dI_{dc}}{dt} = \frac{R_{dc}}{L_{dc}} I_{dc} + \frac{1}{L_{dc}} V_r - \frac{(1-q)}{L_{dc}} V_{dc} \tag{4.21}$$

$$\frac{dV_r}{dt} = \frac{1}{C_0} I_r - \frac{1}{C_0} I_{dc} \tag{4.22}$$

where R_{dc} and L_{dc} are respectively the resistance and the inductance of the boost converter, V_r and I_r are the rectifier output voltage and current,V_{dc} is the dc-link voltage, $0 \leq q \leq 1$ is the duty cycle used to generate the switching signal, and I_{dc} is the inductor current. It must be mentioned that V_{dc}, as a system state, is controlled by the grid currents in our study.

The equations of the L filter in the synchronous reference frame are:

$$\frac{di_{dg}}{dt} = -\frac{R_f}{L_f} i_{dg} + \frac{1}{L_f} v_{di} - \frac{1}{L_f} v_{dg} + \omega_g i_{qg} \tag{4.23}$$

$$\frac{di_{qg}}{dt} = -\frac{R_f}{L_f} i_{qg} + \frac{1}{L_f} v_{qi} - \frac{1}{L_f} v_{qg} - \omega_g i_{dg} \tag{4.24}$$

where R_f and L_f are the resistance and the inductance of the filter, v_{dg} and v_{qg} are the grid voltages, v_{di} and v_{qi} are NPC inverter output voltages, di_{dg} and di_{qg} are the grid currents, and ω_g is the grid angular velocity.

4.3 Controller Design For PMSG Wind Turbine

In order to control PMSG-based WTCS, it is required to generate appropriate switching signals for boost converter and NPC inverter based on the PMSG parameters and connection point requirements. Our proposed sliding mode controller based on EERL considering the first-order dynamics has the following structure:

$$u = g^{-1}(-f + \dot{x}_d - \Lambda S - \frac{K}{D(S)}|S|^{\gamma_x} sign(S)) \tag{4.25}$$

This expression can be applied to every system with governing equation similar to Equation 4.1, considering the availability of inverse of g function. Noticeably, there exists inverse functions of the above-mentioned equations of PMSG-based WTCS components. It is employed to generate duty cycles for boost converter and NPC inverter switches. Based on Figure 4.2, essential input and state vectors are as follows:

$$x = \begin{bmatrix} V_r & I_{dc} & V_{dc} & i_{dg} & i_{qg} \end{bmatrix}^T \tag{4.26}$$

$$u = \begin{bmatrix} q & v_{di} & v_{qi} \end{bmatrix}^T \tag{4.27}$$

where superscript T indicates transposition of the matrix.

As diode rectifier is not a controllable converter, generated power by PMSG can be controlled by I_{dc} (Qiu, Zhou & Li, 2011). To control boost converter, Equation 4.22 is considered. Based on EERL sliding approach, the final control input is:

$$q = -\frac{R_{dc}}{V_{dc}} i_{dc} + \frac{(V_{dc} - V_{dc0})}{V_{dc}} + \frac{L_{dc}}{V_{dc}} \frac{di_{dc-ref}}{dt} - \frac{L_{dc}}{V_{dc}} \Lambda_{dc} S_{dc} - \frac{L_{dc}}{V_{dc}} \frac{K_{dc}}{D_{dc}(S_{dc})} |S_{dc}|^{\gamma_{dc}} sign(S_{dc}) \tag{4.28}$$

where $S_{dc} = i_{dc} - i_{dc-ref}$ and $D_{dc}(S_{dc}) = \alpha_{dc} + (1 - \alpha_{dc})e^{-\beta_{dc}|S_{dc}|}$. In Equation 4.28, V_{dc} has to be controlled such that it is a constant voltage. Desired current of L_{dc} is obtained by MPPT scheme of PMSG. Various MPPT algorithms for PMSG based WECS have been proposed. In this thesis, TSR control is chosen for the MPPT algorithm in which ω_{rm-ref} is obtained using $v_w \lambda_{opt}/R$. Optimum value of TSR is the point that maximizes power coefficient. Commonly, the following generic expression is used to model the WTCS efficiency for extracting mechanical energy from wind kinetic energy (Heier, 2014):

$$C_p(\beta, \lambda) = c_1(\frac{c_2}{\lambda_i} - c_3\beta - c_4\beta^x - c_5)e^{-c_6/\lambda_i} + c_7\lambda \tag{4.29}$$

with

$$\frac{1}{\lambda_i} = \frac{1}{(\lambda + 0.08\beta)} - \frac{0.035}{\beta^3 + 1} \tag{4.30}$$

where the coefficients c_1 through c_7 and x are just the C_p curve fitting coefficients. Consequently, boost converter control diagram method is depicted in Figure 4.3(a).

To control NPC inverter, our goal is to obtain UPF for grid-tied inverter. Hence, quadrature current injected to grid is set to be zero. Considering the L-filter state space, Equation 4.23 and Equation 4.24, the control signals in dq reference frame are expressed as:

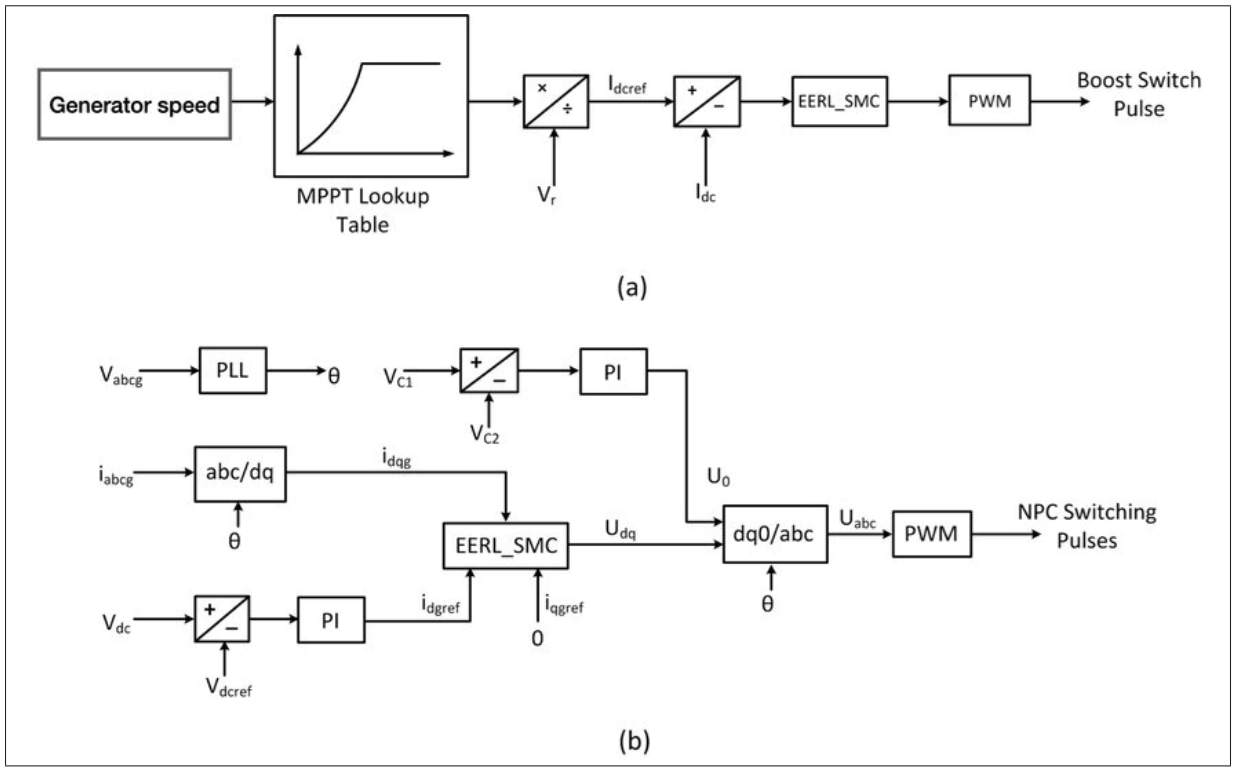

Figure 4.3 SMC-based EERL approach for:
(a) Boost converter control, and (b) NPC inverter control

$$v_{di} = R_f i_{dg} - L_f \omega_g i_{qg} + v_{dg} + L_f \frac{di_{dg-ref}}{dt} - L_f \Lambda_d S_d - L_f \frac{K_d}{D_d(S_d)} |S_d|^{\gamma} sign(S_d) \quad (4.31)$$

$$v_{qi} = R_f i_{qg} + L_f \omega_g i_{dg} + v_{qg} + L_f \frac{di_{qg-ref}}{dt} - L_f \Lambda_q S_q - L_f \frac{K_q}{D_q(S_q)} |S_q|^{\gamma} sign(S_q) \quad (4.32)$$

where $S_d = i_{dg} - i_{dg-ref}$, $S_q = i_{qg} - i_{qg-ref}$, $D_d(S_d) = \alpha_d + (1 - \alpha_d)e^{-\beta_d |S_d|}$ and $D_q(S_q) = \alpha_q + (1 - \alpha_q)e^{-\beta_q |S_q|}$. NPC control approach using SMC based EERL is shown in Figure 4.3(b).

If we suppose that the quadrature component of the grid voltage, v_{qg} is equal to zero, and also having unity power factor, $i_{qg} = 0$, then active and reactive power injected to the grid based on synchronous dq reference frame are $\frac{3}{2} v_{dg} i_{dg}$ and 0, respectively. Therefore, direct and quadrature components control of grid current leads to active and reactive power control of WTCS. This

implies that dc-link voltage must be kept constant and regulated. Desired value of direct-axis current of grid is acquired by PI controller of dc-link voltage.

CHAPTER 5

SIMULATION AND EXPERIMENTAL RESULTS OF PROPOSED SMC CONTROLLER

The goal of this chapter is to validate the performance of the SMC based EERL controller. This chapter includes simulation and experiment of the proposed controller for PMSG equipped wind turbine technology.

5.1 Simulation Results of PMSG Wind Turbine

For verification of the proposed control method in wind energy applications, simulation is performed in MATLAB/Simulink environment. Block diagram of the WTCS, power electronic converters, and proposed controller are shown in Figure 5.1.All signals in this figure are defined in Figures 4.2 and 4.3.

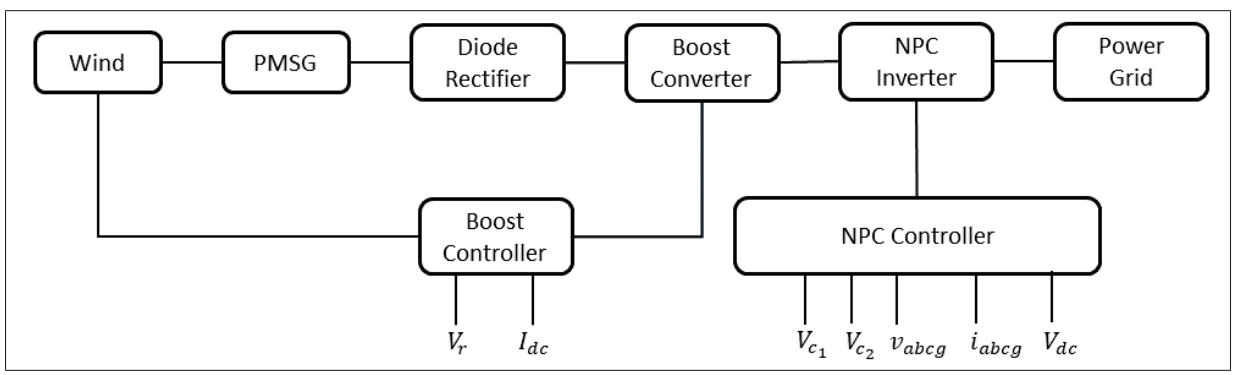

Figure 5.1 General overview of the WTCS and its controllers

Characteristics of WTCS and the proposed control parameters required for the simulation are detailed in Table 5.1 and Table 5.2.

The optimum value of TSR is $\lambda_{opt} = 6.37$. Therefore, the maximum value of power coefficient is $C_{p-max} = 0.4382$, calculated based on $\beta = 0°$ and λ_{opt}. Figure 5.2(a) depicts $C_p(\lambda, \beta)$ using the values of Table 5.1.

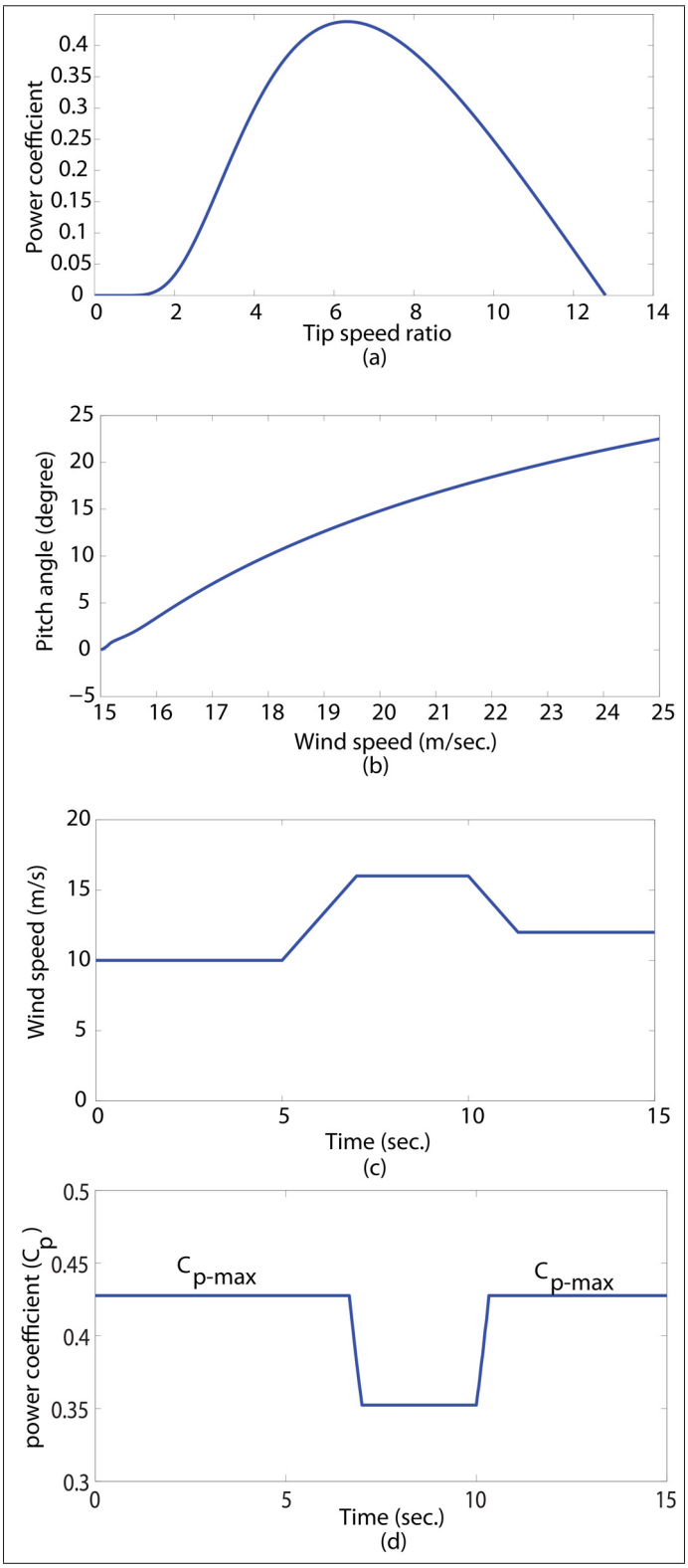

Figure 5.2 Nonelectrical specifications of WTCS: (a) C_p versus TSR curve, (b) Pitch angle curve, (c) Wind profile, and (d) C_p versus time curve

Table 5.1 PMSG-based WTCS parameters

Characteristic	**Symbol**	**Value**
Air Density	ρ	1.225 kg/m^3
Blade Radius	R	1.2 m
Optimal Tip Speed Ratio	λ_{opt}	6.37
Max Power Coefficient	C_{p-max}	0.4382
Inertia	J	0.032 $kg.m^2$
Number of Poles	n_p	10
PMSG Resistance	R_s	0.135 Ω
PMSG Inductance	L_s	4 mH
PM Flux Linkage	λ_f	0.5 $V.s$
Rectifier Capacitance	C_0	1000 μF
Boost Inductance	L_{dc}	1.5 mH
DC Link Capacitance	C_1 and C_2	650 μF (each)
Filter Inductance	L_f	5 mH
Switching Frequency	f_{sw}	2 kHz
Grid Frequency	f	60 Hz
Grid Line Voltage	v_{ab}	$110\sqrt{3}$ V

Table 5.2 PMSG-based WTCS parameters

Coefficients	**Value**
c_1, c_2, c_3	0.22, 116, 0.5
c_4, c_5, c_6	0, 5, 12.5
c_7, x, β	0, 1.5, 0°

Using Equations 2.2, 4.29, and 4.30, a nonlinear function of β and λ is built. Therefore, an iterative nonlinear method can be adopted to solve it for P_T. Figure 5.2(b) shows that how pitch angle adjusts when the wind speed varies.

It is worth noting that due to mechanical limitations in real systems, the pitch angle variation rate should be limited in the range from 3 to 10 $°/s$, based on the wind turbine size (Slootweg, de Haan, Polinder & Kling, 2003). In order to perform simulation, wind speed profile shown in Figure 5.2(c) has been utilized. We suppose that wind speed change is 3 m/s. In the simulation, rated wind speed is 15 m/s and we would like to examine WTCS operation in regions II and III.

Power coefficient C_p of WTCS associated with the wind profile is shown in Figure 5.2(d). It can be seen that when the wind speed is lower than rated value, power coefficient of WTCS is at C_{p-max}. This implies that the wind turbine is operating in MPPT mode. When the wind speed is higher than rated value, power coefficient is decreased to limit the generated power of WTCS to the rated power of wind turbine.

The generated power of PMSG wind turbine and its speed are shown in Figures 5.3(a) and 5.3(b). As it is seen, speed is increased when the wind speed goes up. As a result, electrical power generated by PMSG is increased. It is obvious that when wind speed goes down, speed and power of PMSG are reduced. At $v_\omega = 10$ and $12\ m/s$, which are less than rated wind speed, pitch angle is set to $0\ ^\circ/s$ to let the WTCS extract all the available energy from the wind. Clearly, PMSG power is less than nominal power of the system. In contrast, at $v_\omega = 16m/s$, which is greater than rated wind speed, pitch controller modifies the pitch angle based on Figure 5.2(b) to reduce the amount of power harvested by WTCS, therefore, generator speed is controlled at its rated speed and $4\ kW$ is generated by the wind turbine. Whereas the generator power is controlled by I_{dc} , their waveforms have the same shape characteristics.

Figure 5.3(c) depicts waveforms of dc-link voltage V_{dc} and dc-link capacitors voltages V_{C_1} and V_{C_2} . dc-link voltage has been greatly controlled to be kept constant at $400\ V$. When there is a change in wind speed, a small variation is observed in dc-link voltage. As it is obvious, the controller regulates it very fast. As voltages of C_1 and C_2 cannot be easily distinguished in Figure 5.3(c), initial part of the figure is highlighted to show it clearly. After $t = 0.17s$, capacitor voltages are balanced even in the presence of wind speed variation.

The target of grid-connected renewable energy system such as WTCS is to transfer maximum power into the grid with UPF because poor power factor on the power network increases power line losses and makes it very difficult to keep the voltage regulated. Voltage and current waveforms of phase (a) at PCC as well as a closer observation of them are demonstrated in Figure 5.4.

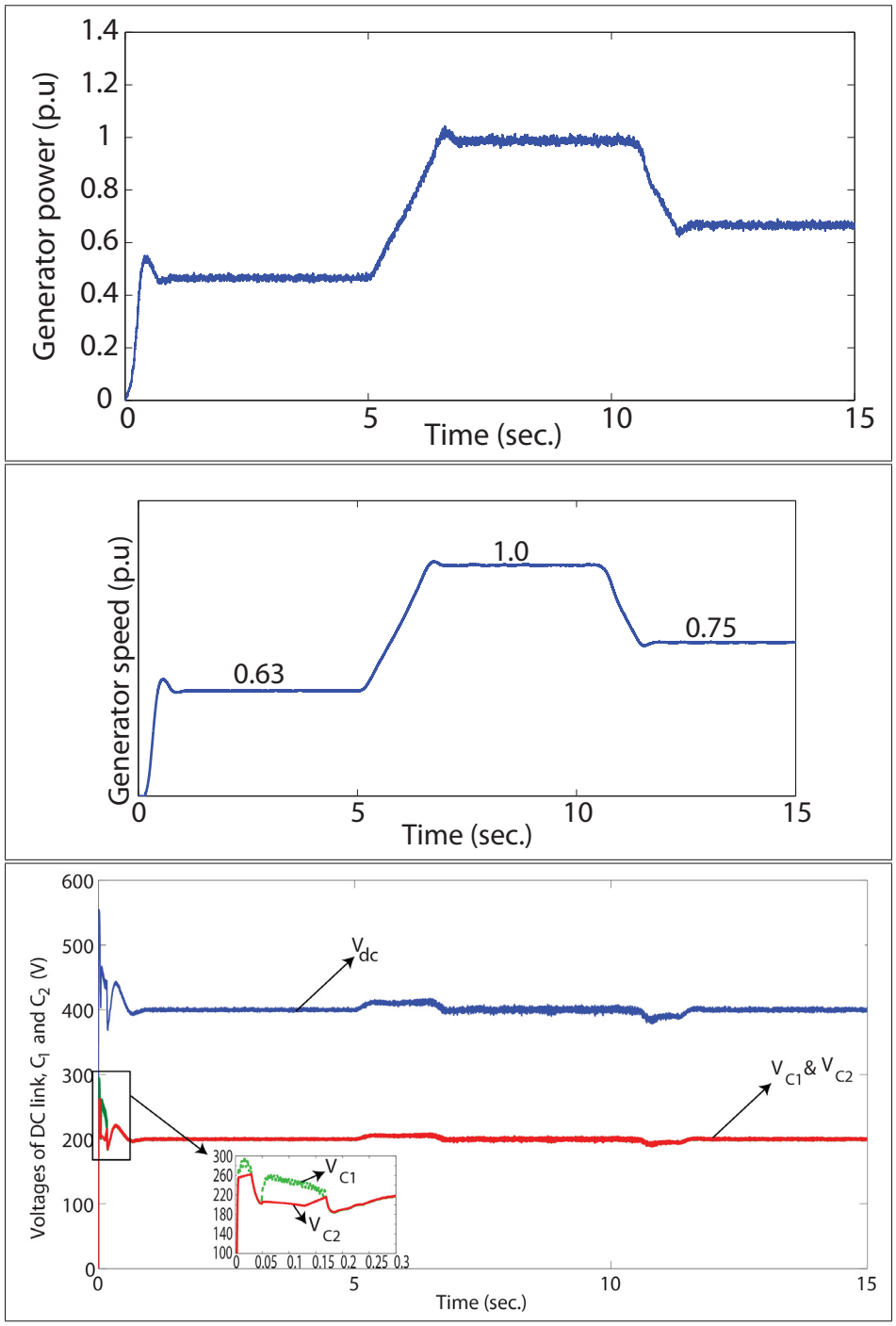

Figure 5.3 Waveforms of: (a) PMSG power, (b) PMSG speed, and (c) dc link, C_1 and C_2 voltages

It should be noted that current waveforms have been enlarged and multiplied by a constant number to be seen more easily. One salient objective of the controller in WECS is to obtain

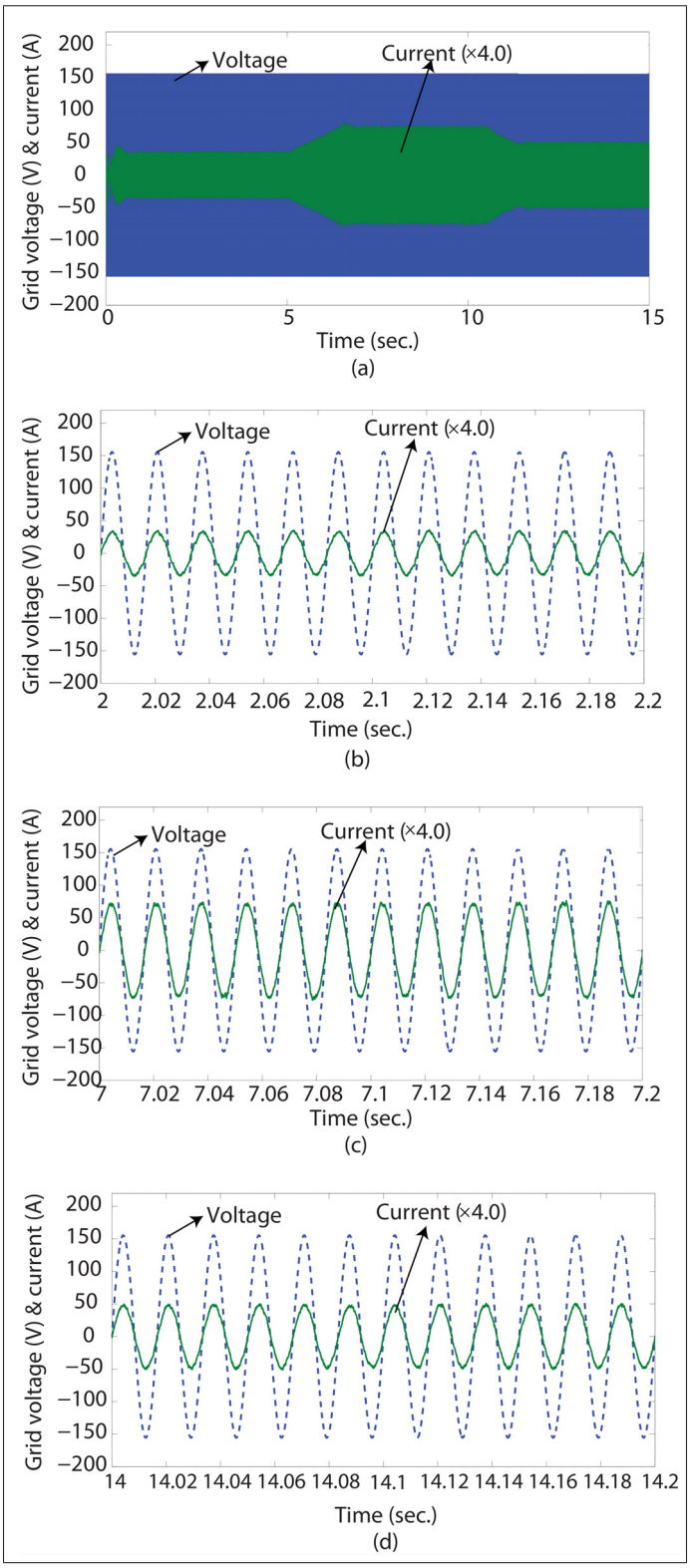

Figure 5.4 Voltage and current waveforms of phase (a) at PCC in the ranges: (a) $0 \leq t \leq 15$, (b) $2 \leq t \leq 2.2$, (c) $7 \leq t \leq 7.2$, and (d) $14 \leq t \leq 14.2$

UPF. From Figure 5.4, it is clear that in steady state, current at the grid is in phase of voltage at all wind speeds. Since wind speed change rate is set at $3m/s$, there is no instantaneous variation of current at PCC. There exists UPF even during variation of wind speed.

Figure 5.5 compares the chattering perspective of EERL and ERL methods. It is distinct that EERL method mitigates the chattering issue more than ERL approach.

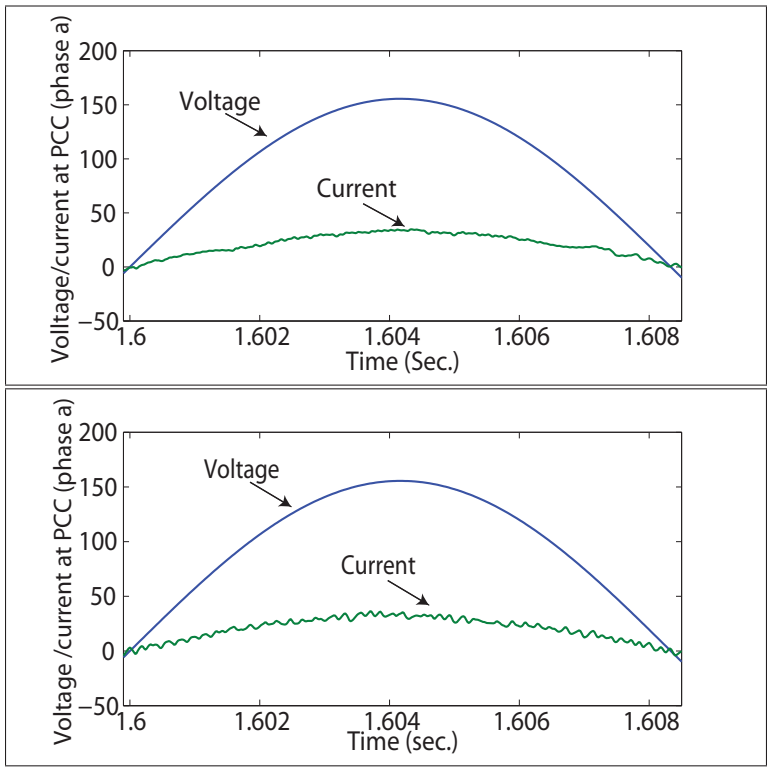

Figure 5.5 Comparison of chattering issue of: (a) EERL method and (b) ERL method

One major impediment of diode rectifier in PMSG wind turbine is the high harmonic contents in the generator stator current which leads to the generator torque and dc-link voltage ripples. Ripple in dc-link voltage is smoothed by incorporating capacitor C_0 between the diode rectifier and the boost converter. Several studies have been directed to minimize the PMSG torque ripple connected to diode rectifier (Xia, Wang, Shi & Song, 2013; Xia, Fletcher, Finney, Ahmed & Williams, 2011). Nonetheless, it must be devised to design the PMSG and related drive-train in such a way that they could tolerate generator torque ripple (Wu *et al.*, 2011; Xia

et al., 2011). Simulation results show that the maximum electromagnetic torque ripple of PMSG is approximately 0.17 per unit.

5.2 Experimental Results

For validation of proposed SMC-based EERL method, a laboratory prototype according to Figure 5.6 is implemented to evaluate proposed controller in which V_{dc} is a variable dc source. It should be noted that this structure has been chosen for controller validation purpose due to the laboratory setup limitations. Scheme used in Figure 5.6 and applied controller can also be employed for grid integration of other types of renewable energy. By replacing the PMSG, MSC, and dc bus with a dc source, dc-link ripples are slightly ignored. Hence, voltage ripples of capacitors C_1 and C_2 are a little less than real system but the variation of dc-link voltage is examined in the experiment along with the balancing challenge of the voltages V_{c_1} and V_{c_2} . In our setup, clamping diodes and MOSFETs types are SCT2080KE and SCS220KG, respectively. dSPACE DS1103 real-time controller board is employed to implement the SMC-based EERL with $20\mu s$ sampling rate. This hardware encompasses a processor and some I/Os to be able to accomplish the control procedures. Real-time interface of dSPACE lets us implement the Simulink and Stateflow models on the hardware. The experimental setup data is given in Table 5.3.

Table 5.3 PMSG-based WTCS parameters

Characteristics	**Value**
DC link voltage	$300\ V$
C_0	$1000\ \mu F$
L_{dc}	$1.5\ mH$
C_1 and C_2	$650\ \mu F$
L_f	$5\ mH$
Switching frequency	$2\ kHz$
Grid frequency	$60\ Hz$
Grid line voltage	$100\sqrt{3}\ V$

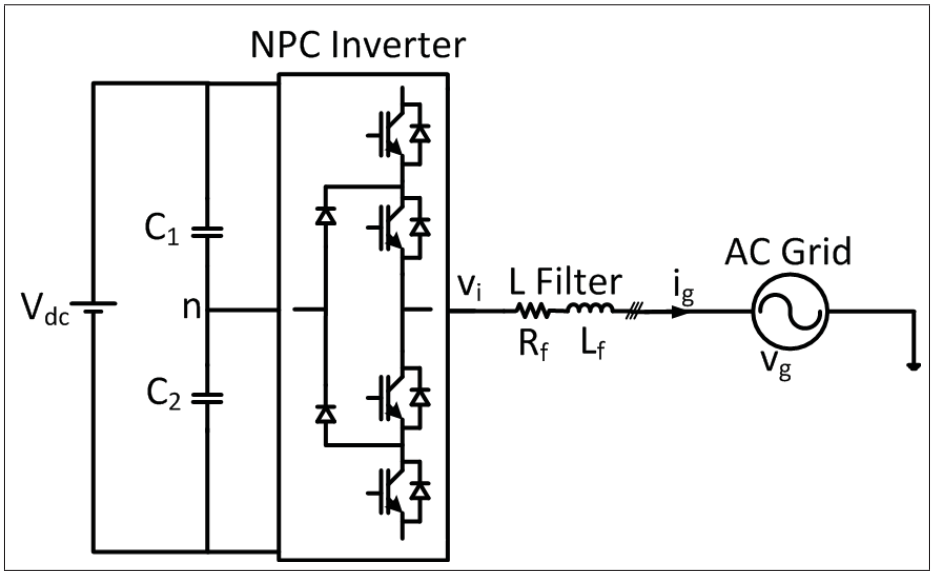

Figure 5.6 Experimental set-up scheme

To explore the effectiveness of proposed method, it is compared with SMC-based ERL and PI approaches. Figures 5.7, 5.8, and 5.9 show the set-up results including the NPC inverter and L filter using EERL, ERL, and PI approaches, respectively, in which V_{c_1}, NPC output line voltage, and PCC voltage and current (phase a) are shown. Control parameters for EERL method are the same as parameters used in simulation, listed in Table 5.4. For ERL approach, parameters are as follows: $\alpha_d = \alpha_q = 0.1$, $\beta_d = \beta_q = 10$. Parameters associated with PI method are as follows: $K_p = 19.25$, $T_i = 0.01$ (current control), and $K_p = 0.95$, $T_i = 0.02$ (dc-voltage control). These parameters are obtained such that we meet the requirements of settling time 1.2 ms and overshoot 5.1%. Since a grid-connected NPC inverter is tested at this point, the main objectives are to reduce chattering phenomenon, to balance voltage of capacitors C_1 and C_2, to obtain UPF, and to achieve permissible harmonic level with low-power losses and low switching frequency.

The five-level voltage waveform between phases (a) and (b) of the NPC inverter output, v_{ab_i} in Figures 5.7(a), 5.8(a), and 5.9(a) demonstrate that the dynamic performance of the EERL approach is more smooth than the ERL and PI methods. Moreover, low-voltage ripple of V_{C_1} as well as voltage balancing depicted in these figures prove that the controller has been properly designed and applied to the system. Voltage of capacitor C_1 in all applied techniques is about

Table 5.4 SMC based EERL parameters

Characteristics	Value
Λ_{dc}, Λ_d and Λ_q	75, 50, 50
K_{dc}, K_d and K_q	200, 100, 100
α_{dc}, α_d, α_q	0.3, 0.4, 0.4
β_{dc}, β_d and β_q	10, 5, 5
γ_{dc}, γ_d and γ_q	0.1, 0.1, 0.1

150 V, half of the dc-link voltage (V_{dc} = 300V). Figures 5.7(b), 5.8(b), and 5.9(b) illustrate an increase of dc-link voltage from 300 to 330 V for three methods in which V_{C_1} of EERL coincides with V_{C_2} with lowest deviation and ripple during transients.

In the IEEE standard for harmonic control in electrical power systems IEEE Std 519, allowable THD at PCC must be less than 5%. AMEC power analyzer has been used to capture voltage and current waveforms of the connection point to the grid to analyze THD of waveforms. Figure 5.10 highlights one cycle of voltage and current at PCC. From Figure 5.10, it is clear that all three methods have acceptable performance regarding THD of the current waveform. But it is observed that THD value obtained by EERL is 1.9% which is much smaller than THD of ERL (3%) and PI (3.5%) methods. It should be noted that by choosing aforesaid PI parameters for current controller, EERL outperforms PI method.

It is obvious that the power factor in PI, ERL, and EERL methods is almost 1 and, therefore, the reactive power injected to the grid through the NPC inverter is near zero. Power electronic converter designers consider the voltage ripple of dc-link capacitors to be a key aspect in their design considerations. It can be deduced from experimental results that peak to peak voltage of capacitor is detracted by EERL method in comparison to ERL and PI methods.

Finally, to verify the dynamic response of the SMC-based EERL controller on the grid-tied NPC inverter in renewable energy applications considering input power variations, step changes in input power amplitude have been exerted to the set-up input. Figure 5.11 shows the results for this case. Figure 5.11(a) shows a decrease of dc-link voltage from 330 to 290 V and again up to 330 V, and Figure 5.11(b) demonstrates step changes in current reference from 5 to 8 A.

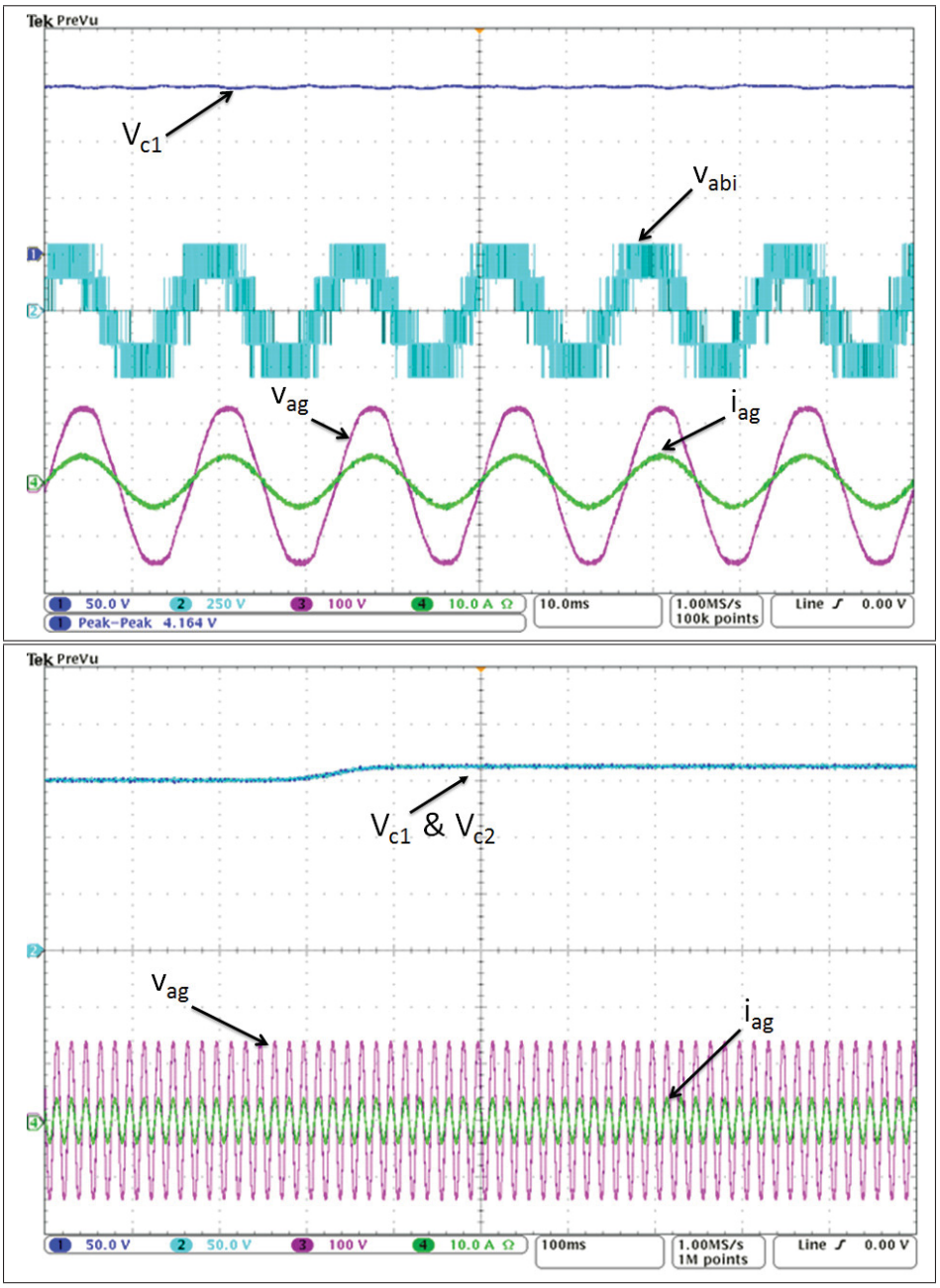

Figure 5.7 Voltage of capacitor C_1 , NPC voltage, and current and voltage waveforms of phase (a) at PCC using SMC-based EERL in: (a) steadystate mode, and (b) transient mode

It is evident that the proposed controller takes proper action in the short period of time to keep UPF operation throughout the working regions with different input powers, and to maintain the dc-link voltage well-tracked its reference as well as to generate high-quality power at PCC.

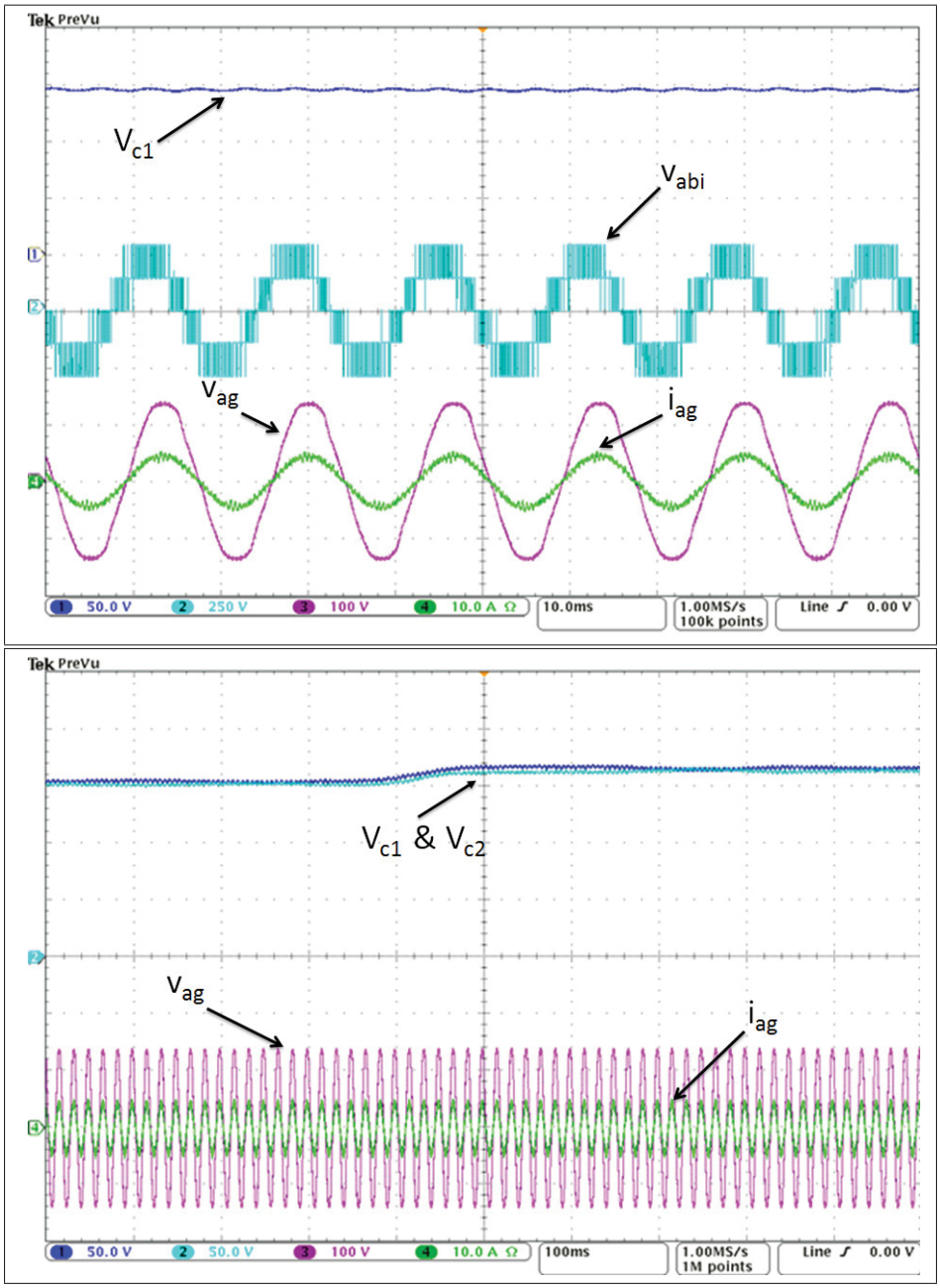

Figure 5.8 Voltage of capacitor C_1, NPC voltage, and current and voltage waveforms of phase (a) at PCC using SMC-based ERL in: (a) steady-state mode, and (b) transient mode

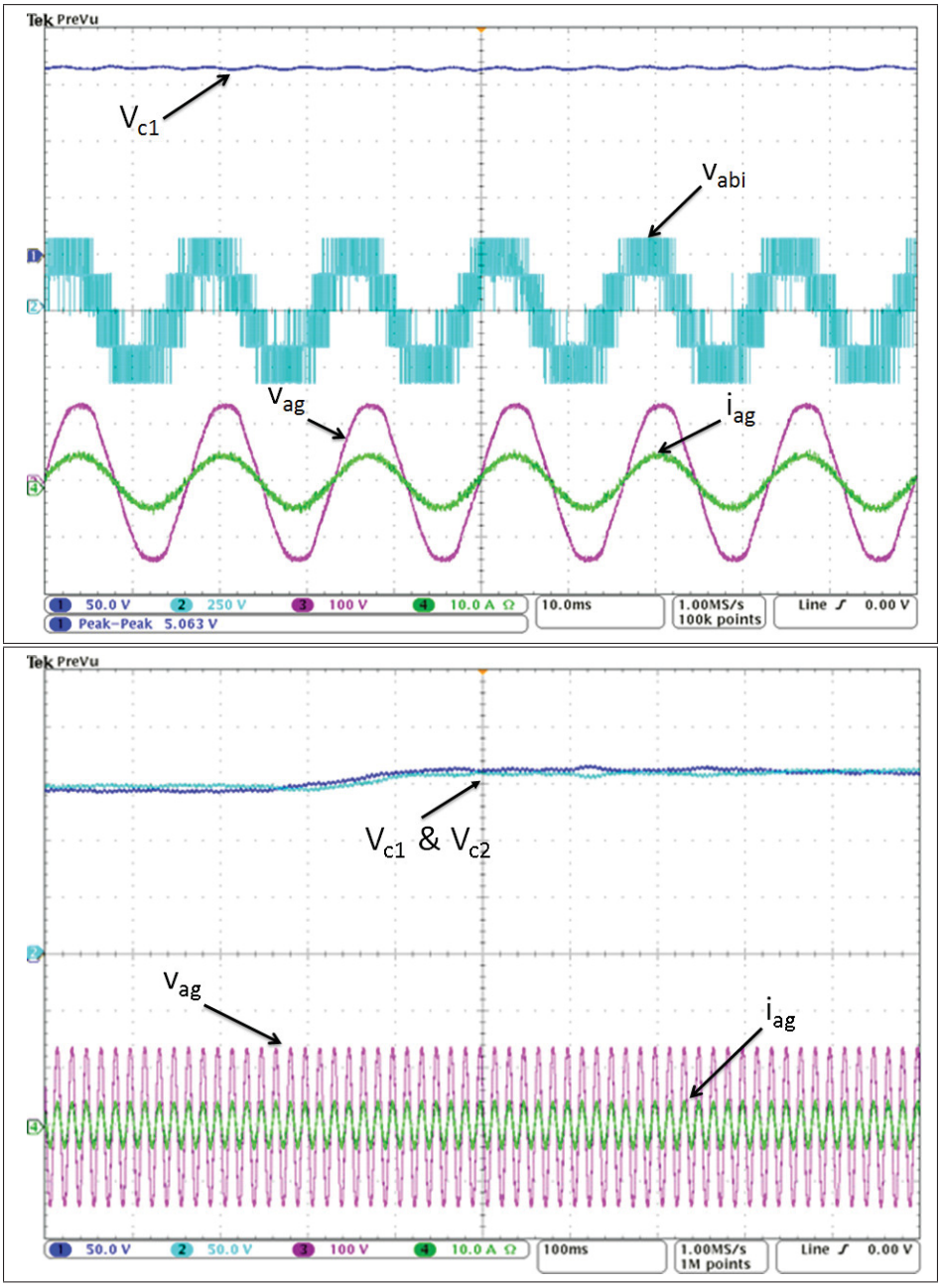

Figure 5.9 Voltage of capacitor C_1, NPC voltage, and current and voltage waveforms of phase (a) at PCC using PI approach in: (a) steady-state mode, and (b) transient mode

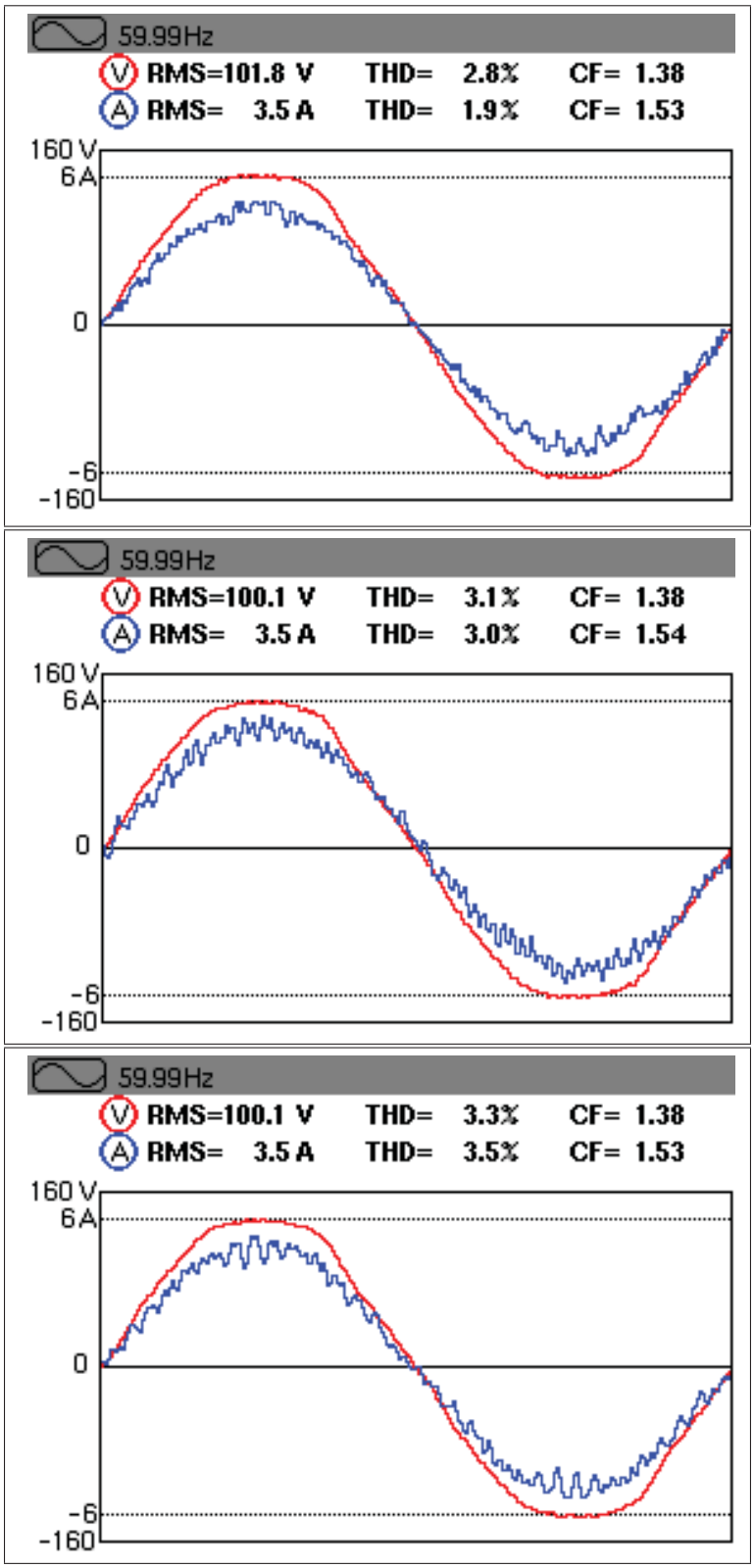

Figure 5.10 Comparison of EERL, ERL, and PI methods based on THD of the currents injected to the grid: (a): EERL, (b): ERL, and (c): PI

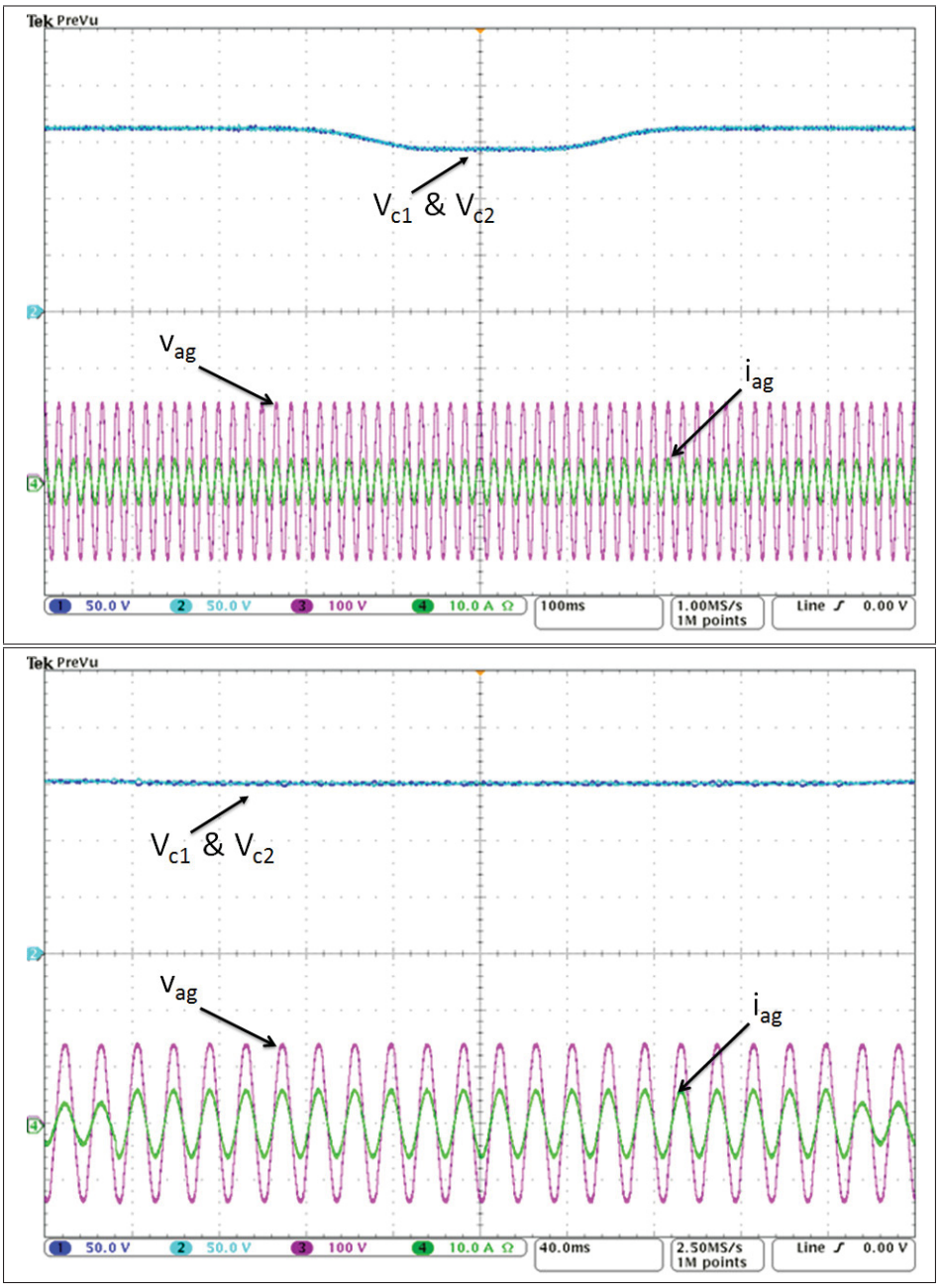

Figure 5.11 Voltage and current waveforms at PCC: (a) V_{dc} alters in two levels of voltages: 330 and 290 V and (b) PCC reference current changes from 5 to 8 A

CHAPTER 6

FAULT DETECTION OF PMSG WIND TURBINE USING GEOMETRIC APPROACH

The goal of this chapter is to propose a model-based Fault Detection and Localization (FDL) strategy of a surface-mounted Permanent Magnet Synchronous Generator (PMSG) Wind Turbine Conversion System (WTCS). One of the prevalent faults in wind turbines is Inter-turn Short Circuit (ISC) fault in the generator of WTCS. To elaborate the fault and observe the consequences, a 120 KW wind turbine equipped with PMSG is being modeled while injecting the fault during normal and steady state operation. Geometric Approach (GeA) offers plentiful features for FDL in nonlinear system control applications. It can operate as a built-in function of the WTCS control system in which ISC fault is being detected and localized when occurred in the winding of the stator of PMSG. The GeA is a model-based technique that works based upon the governing equations of the generator of wind turbine. In this chapter, we will be using the PMSG model in abc reference frame developed in Chapter 3.

6.1 Geometric Approach (GeA)

The FDL algorithms in the complex dynamic systems have been extensively probed over the last decades. One of the promising methods relying on system model is GeA. General form of GeA for FDL of linear and nonlinear systems is elaborated in (Massoumnia, 1986; Persis & Isidori, 2001). The fundamental concept of this approach is to form a subsystem in which faults can be detected while disturbances are decoupled and isolated as well. In geometric approach, at first, inverse dynamic of the system is constructed using input and output measurements. Then the unknown input to the system (fault) is reconstructed as shown in Figure 6.1.

Here, we briefly explain the structure of geometric approach and provide the formulas for fault detection purposes. It is supposed that dynamic of the system is represented by the following equation:

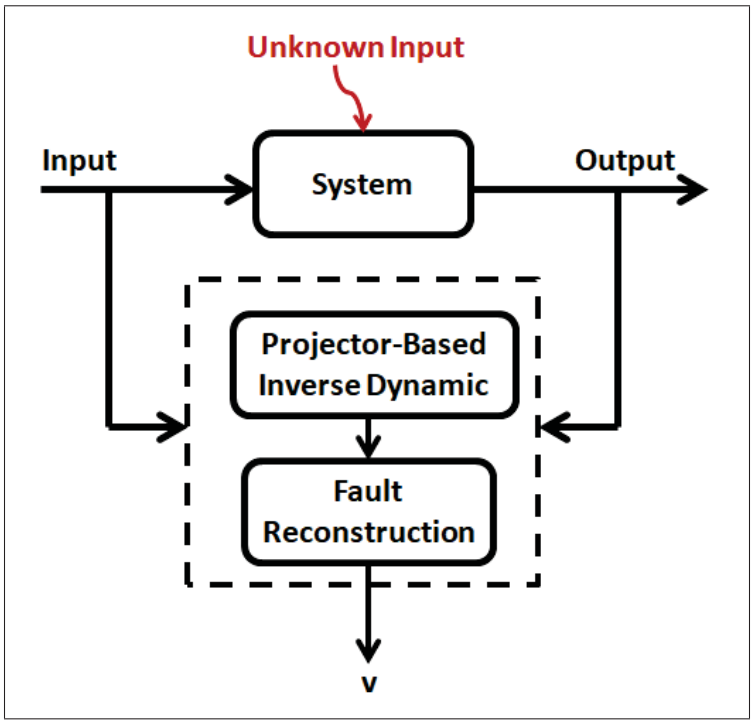

Figure 6.1 General overview of geometric approach

$$\begin{cases} \dot{x} = f(x) + Bu, Bu = \sum_{i=1}^{m} b_i(x)u_i \\ y_j = h_j(x), 1 \leq j \leq p \end{cases} \tag{6.1}$$

where x, u, y, and B are state, input, output vectors, and input matrix respectively. Note that m and p represent the order of inputs and outputs of the system. All functions in Equation 6.1 are supposed to be smooth in order to have continuous derivatives up to the required order over their domain. We define following matrix:

$$\begin{cases} \sigma = [\sigma_1, ..., \sigma_p] \\ \sigma_j = L_f^{r_j - 1} h_j, 1 \leq j \leq p \end{cases} \tag{6.2}$$

where $L_f^{r_j-1}$ is the $(r_j - 1)^{th}$ Lie derivative of h_j with respect to the vector f, and r_j is the relative degree of h_j. In fact, it will quantify the changes of h along the vector f. Then, the gradient of matrix σ is given by:

$$\nabla\sigma = [dL_f^{r_1-1}h_1, ..., dL_f^{r_p-1}h_p] \tag{6.3}$$

Let us assume the following definition for Matrix A:

$$A = \nabla\sigma^T B \tag{6.4}$$

where superscript T stands for the transpose. To be able to use the GeA for specified application, the following conditions have to be satisfied:

1. $rank(A) = m$.
2. for $1 \leqslant j \leq p$, $dL_f^{r_j-1}h_j$ are linearly independent.

When the number of inputs is greater than or equal to the number of outputs, a standard GeA can be utilized for the fault detection aim. Based on the Equation 3.12, the standard GeA seems to be well suited for the WTCS application without the need of further modification. Based on (Chaib, Boutat, Benali & Kratz, 2009), a geometric projector can be defined as:

$$\Pi = I_n - LA^{-1}\nabla\sigma^T \tag{6.5}$$

By defining $W = \dot{y}$ and using previous equations, the inverse dynamic of the system and fault reconstructed matrix are given as:

$$\begin{cases} \dot{x} = \Pi f + LAW \\ v = A(W - \nabla\sigma^T f) \end{cases} \tag{6.6}$$

For those who need more information regarding the details on the GeA, they can refer to the references provided in this paper and the references therein.

6.2 Inter-turn Short Circuit (ISC) Fault Modeling

Several studies have been done to provide an analytical model for ISC fault in the winding of the electrical machines such as (Cintron-Rivera, Foster & Strangas, 2015; Jeong, Hyon & Nam, 2013; Vaseghi, Takorabet & Meibody-Tabar, 2009). The validated analytical model with embedded inter-turn fault is depicted in Figure 6.2. In this figure, resistor R_f in the model is used for fault injection and represents the fault intensity in the generator winding. When $R_f \rightarrow 0\ \Omega$, it indicates that the insulation of the short-circuited turns has been damaged thoroughly. When R_f takes a positive amount (Ω), it shows that an incipient fault is occurring in the winding. And finally, $R_f \rightarrow \infty$ describes a healthy system without ISC fault.

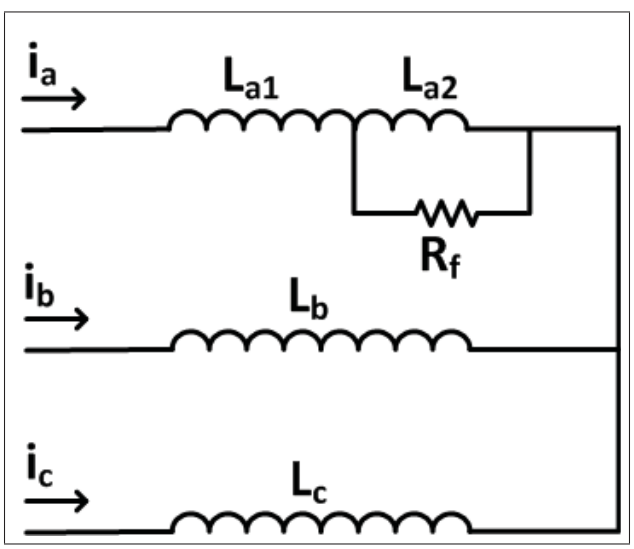

Figure 6.2 Equivalent model of PMSG including inter-turn short circuit fault

To have a more realistic model of a PMSG wind turbine, we use Ansys software version 19 to obtain the Finite Element Model (FEM) of the generator while applying an ISC fault in the phase a of PMSG. In this paper, parameters of a 120 KW PMSG shown in Table 6.1 are being used to simulate the wind turbine generator using Ansys software.

Table 6.1 Simulation parameters of a 120 KW PMSG

Characteristics	**Value**
Power	120 KW
Rated Voltage	200 V
Rated Speed	100 rpm
Number of Poles	32
Number of Slots	168
Rotor Outer Diameter	1798 mm
Rotor Inner Diameter	1650 mm
Stator Outer Diameter	1600 mm
Stator Inner Diameter	1300 mm
Length	140 mm
Steel Type	$M19-24G$
Magnet Type	$XG196/96\ mm$

To avoid the complexity of creating the geometry of PMSG in Ansys Maxwell 2D, we begin initially with Ansys RMxprt which is a template based platform to expedite the design of electric generator for developing its FEM model. Rotor, stator, slot, winding, and permanent magnets parameters and dimensions of PMSG have to be specified in RMxprt. It is worth noting that RMxprt automatically sets up a reduced order model of the machine.

In the next step, we have to import our design features used in RMxprt to Maxwell 2D. The major advantage of RMxprt is its capability to automatically create a whole Maxwell 2D project comprising geometry, materials and boundary conditions. Here, we also have the reduced order model. Since we are going to apply an ISC fault, a full Maxwell 2D model of PMSG is required for the analysis goal. The process to form an ISC fault is depicted in Figure 6.3.

The last step is to create the FEM model of the faulty generator. Indeed, the faulty model can be acquired by modification of healthy model generated with Maxwell 2D. As a matter of fact,

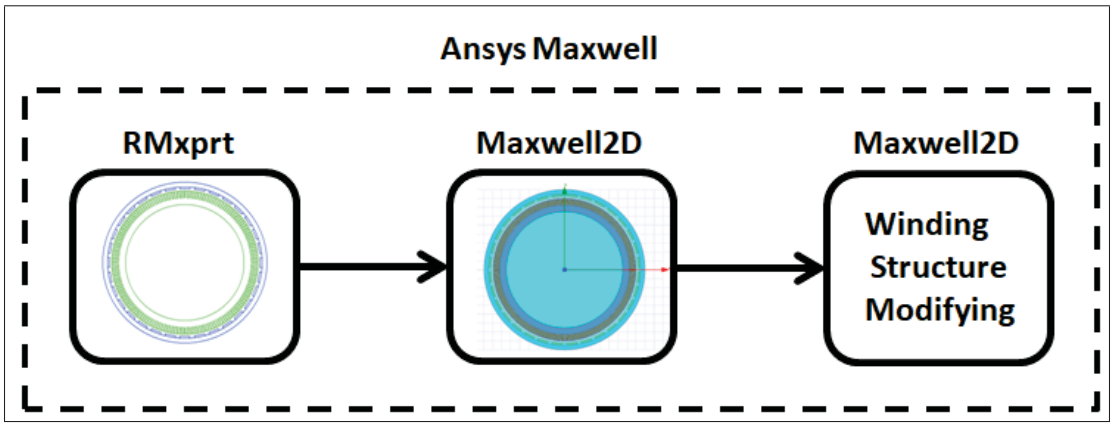

Figure 6.3 Procedure of applying the inter-turn short circuit fault of a PMSG wind turbine

faulty model has an extra coil respect to the healthy model to mimic the short circuit loop shown in Figure 6.2. The healthy generator modeled in this paper has 56 slots per phase, 28 coils per phase, and 17 conductors per slot. Considering that if the whole turns of a coil in one phase are short-circuited, that phase includes 27 healthy coils as well as a faulty coil. Suppose that 3 turns of a coil in one phase are short-circuited, in this situation that phase consists of 27 healthy coils each 17 turns, and one coil with 14 intact turns and 3 short-circuited turns. For creating the faulty model in the second scenario, a new coil with 3 turns constitutes a new phase in Maxwell 2D. Now, we have access to the short-circuited turns of the coil through a new phase created in the model.

6.3 Co-Simulation of PMSG With Inter-turn Short Circuit (ISC) Fault

For this study, simulations have been carried out to prove the validity and strength of the geometric approach for ISC fault detection and localization of PMSG equipped wind turbine. The simulation structure, called co-simulation, is shown in Figure 6.4. As seen in this figure, we are using 3 software packages whose are Matlab/Simulink, Simplorer, and Maxwell to run the simulation. Control system as well as the FDL method are designed in Matlab, while FEM modeling of the machine is the duty of Maxwell. In order to connect the control scheme to the

generator, an interface, Simplorer software is required to accomplish the task. Simplorer which is a trademark of Ansys, is an electronic circuit analysis software.

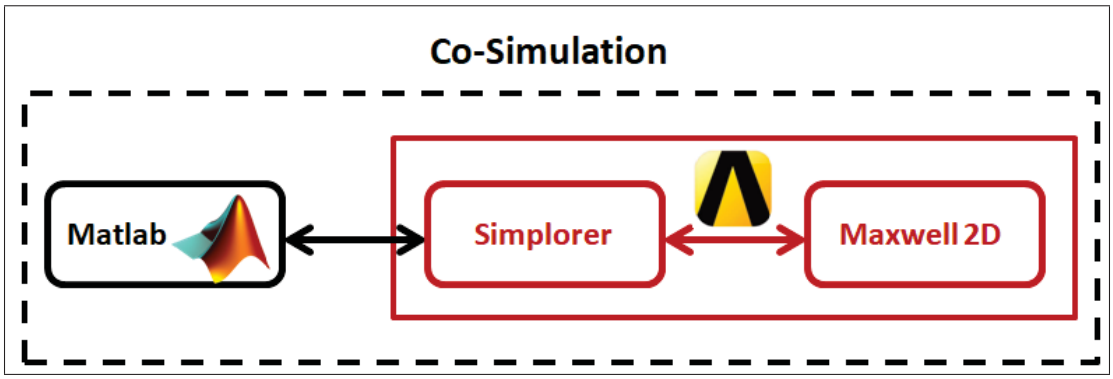

Figure 6.4 Co-simulation setup for analyzing the PMSG wind turbine with faulty coil

Since we would like to analyze ISC fault at its incipient stage with minimum turns involved, one turn of a coil in phase a are short-circuited using R_f with different values, 0 Ω, 2 $m\Omega$, and 20 $m\Omega$. Number of conductors per slot in this machine is 17. It is noteworthy that running the co-simulation takes a lot of time to be completed because we cannot use the symmetry to process the ISC fault in the machine and decrease the simulation time. The time step for the co-simulation is 20 μs and it is run for 2 seconds to be able to analyze the machine behavior after passing the transient period due to the inertia of the PMSG. The current waveform of phase a of the healthy generator connected to the grid is shown in Figure 6.5. This figure just demonstrates a short period of time in the steady state situation.

At one point in the simulation, an ISC fault is injected in the phase a of the PMSG winding. The current waveform flowing in the short-circuited turn of one coil with different fault intensity is shown in Figure 6.6. The fault injection is applied when the generator is operating in its steady state mode.

To have a better understanding of the faulty situation, Figure 6.7 depicts the difference between phase a current and the current inside the short-circuited turn. Figure 6.6 and Figure 6.7 clearly

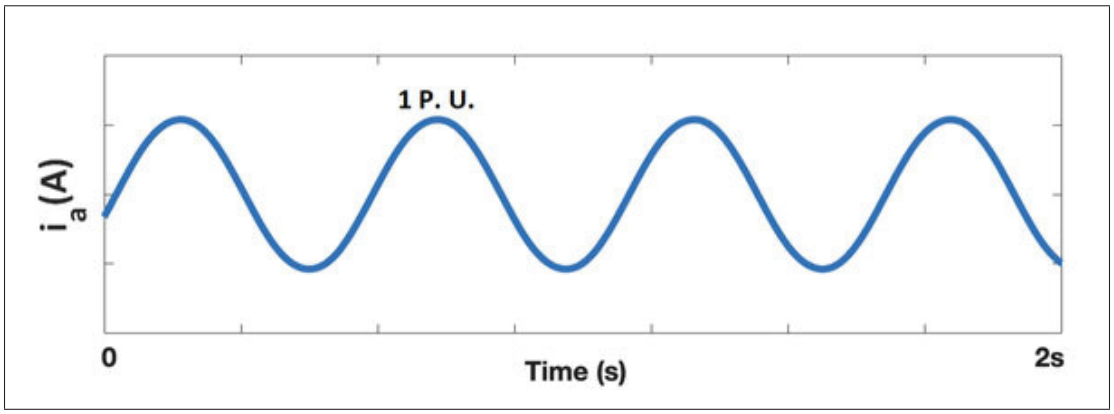

Figure 6.5 Healthy generator current of phase (a)

show that the maximum circulating current is flown in the short-circuited loop in the case of $R_f = 0\ \Omega$, meaning the complete damage of the insulation of that turn.

In order to run the co-simulation with its controller up and running, data has to be transferred between Matlab and Ansys. Required signals for control purpose are demonstrated in Figure 6.8. Parameters specially needed for the FDL control system are generator voltages, currents, and speed.

As the ISC fault with $R_f = 20\ m\Omega$ has the minimum circulating current between all faulty scenarios, we choose that situation to check the sensitivity and ability of the FDL scheme for detecting the fault and its location. Although ISC faults create high current in the short-circuited turns, they cannot be easily detected from generator phases currents (Zafarani, Bostanci, Qi, Goktas & Akin, 2018). The co-simulation results verify that the faulty scenario cannot be readily distinguished from healthy situation too. Figure 6.9 shows the output of FDL controller for different phases.

As it is obvious from Figure 6.9, the geometric approach FDL scheme detects the ISC fault injected in phase a of the PMSG in the short period of time (around 320 ms). To show the effectiveness of the FDL method, we applied the short circuit fault with just one turn involved as well as a resistance of $R_f = 20\ m\Omega$ for representation of incipient and small fault intensity.

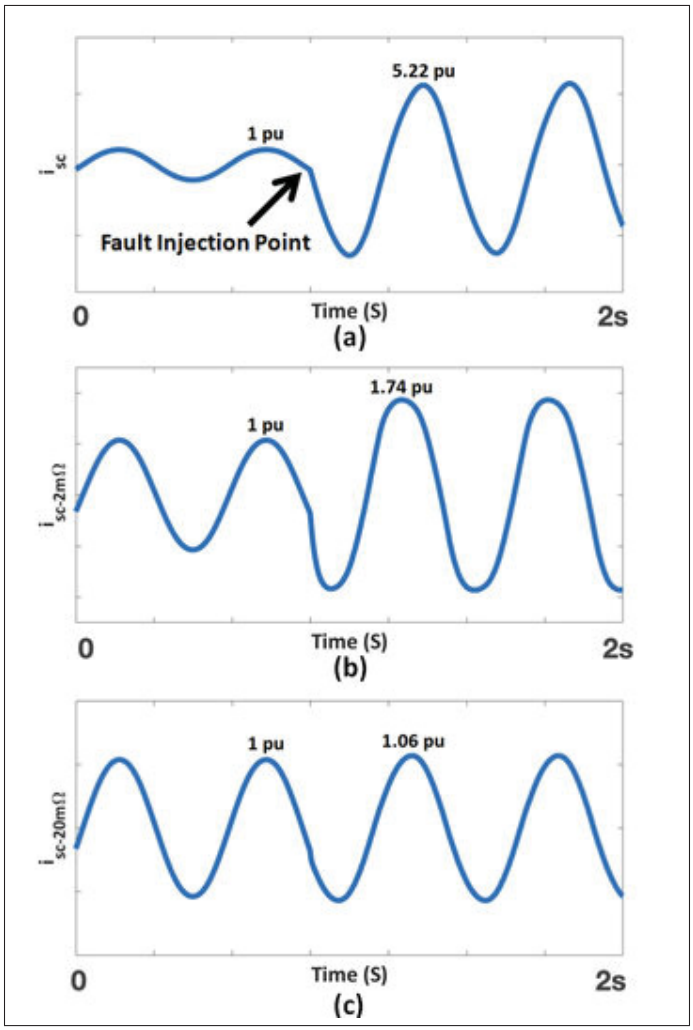

Figure 6.6 Faulty phase (a) current with: (a) $R_f = 0\Omega$, (b) $R_f = 2\ m\Omega$, and (c) $R_f = 20\ m\Omega$ respectively

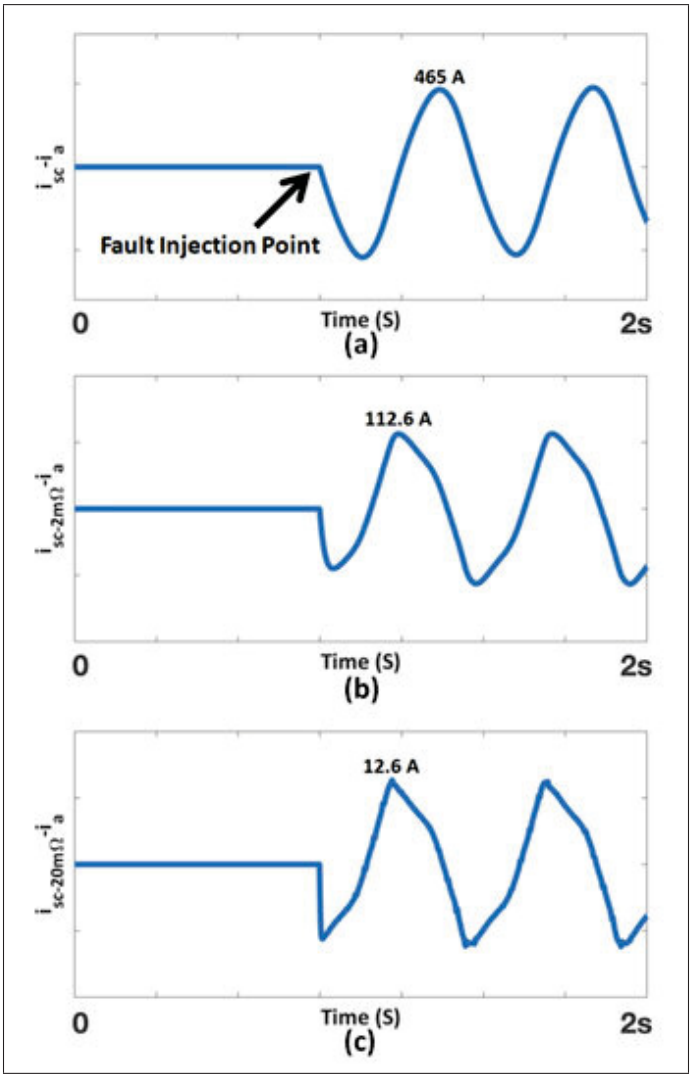

Figure 6.7 Difference between phase (a) current and short-circuited turns current with: (a) $R_f = 0\ \Omega$, (b) $R_f = 2\ m\Omega$, and (c) $R_f = 20\ m\Omega$ respectively

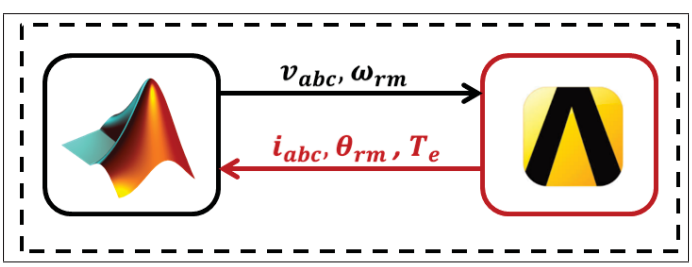

Figure 6.8 Data transfer diagram between Matlab and Ansys

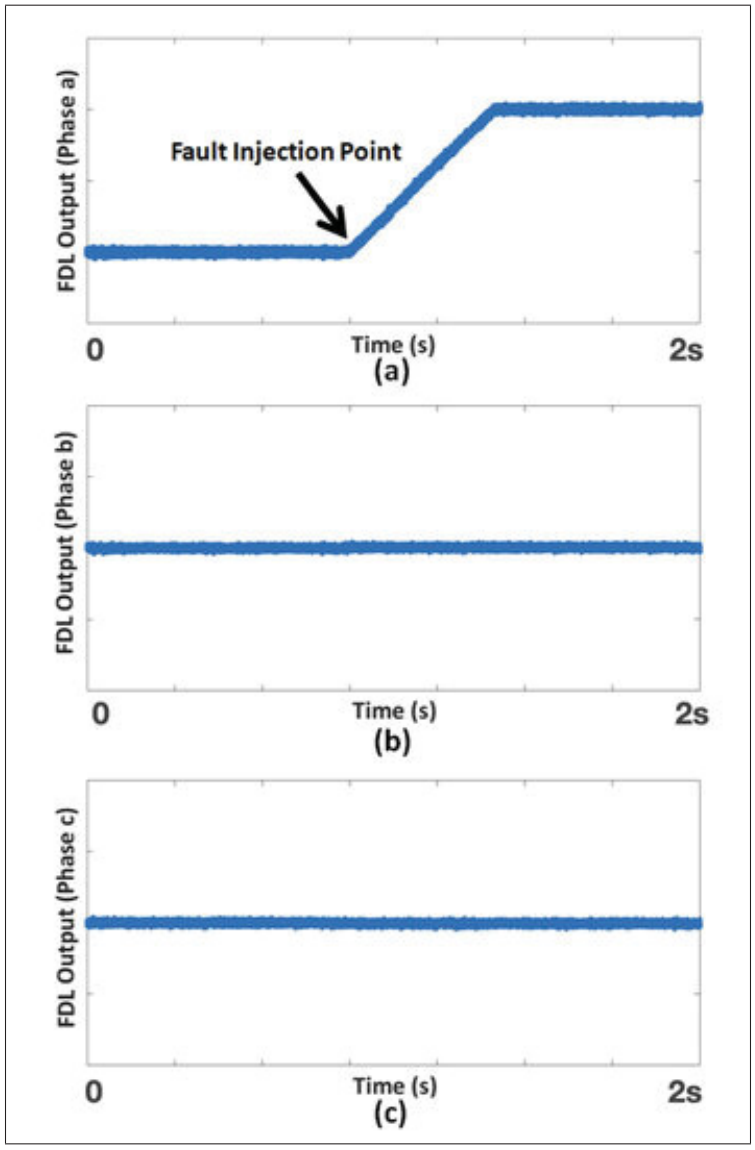

Figure 6.9 The output of FDL controller for three phases while having an inter-turn short circuit fault in phase a with $R_f = 20\ m\Omega$

CONCLUSION AND RECOMMENDATIONS

This chapter provides the approaches used in this thesis to design an advanced controller for WTCS and fault detection strategy of the PMSG. It includes the following two sections:

1. Contributions and achievements are explained in the first section.

2. Possible recommendations are provided in the second section.

7.1 Conclusion

In Chapter 4, a SMC based on EERL was proposed and investigated on the grid-connected PMSG wind turbine system. The examined topology consists of: diode rectifier, boost converter, NPC inverter, and L filter. This topology can be used in low-power and medium-power wind turbine systems. Boost converter is controlled by MPPT idea of PMSG, while NPC inverter control is developed using the UPF concept. The key features of the proposed controller are: chattering minimization respect to conventional and ERL sliding mode controllers, proper voltage balancing performance of dc-link capacitors, improving transient traits of WECS, and appropriate dynamic error tracking. The verification of the proposed reaching law for SMC approach was validated by both simulation and experiment.

In Chapter 6, we proposed and examined a Fault Detection and Localization (FDL) scheme to detect an Inter-turn Short Circuit (ISC) fault of a wind turbine when it is in incipient stage. The wind turbine system equipped with a Permanent Magnet Synchronous Generator (PMSG) is connected to the power grid. The suggested FDL method is based on Geometric Approach (GeA) which is a powerful tool for fault detection of complex nonlinear system. The main attributes of FDL using geometric method are: being a model-based strategy operating on governing equation of the system, detection of fault at its early advent, providing the fault location, remaining insensitive to system parameter changes, and processing the procedure in short period of time.

The validation of proposed FDL technique was performed by the co-simulation of wind turbine using Maxwell, Simplorer, and Matlab software packages.

7.2 Recommendations for Future Works

In this thesis, we proposed an advanced controller for PMSG equipped WTCS and inter-turn fault detection of PMSG wind turbine. Pursuing this research, following recommendations for diving deeper and extending this work are:

1. The control strategy proposed in Chapter 4 was applied on PMSG equipped wind turbine with NPC converter. The proposed method can be examined on other common power electronic technologies in the wind industry.

2. Average wind speed profile was used in Chapter 4 to develop the EERL control strategy. Variation of wind speed and its effect on the operation of wind turbine can be explored.

3. Fault detection algorithm based on geometric approach developed in Chapter 6 just focused on the detection of inter-turn short-circuited fault in one phase. Therefore, detection of two simultaneous faults in different phases can be analyzed.

4. A non-planned service can be highly expensive because many wind turbines are installed offshore. So, fault tolerant control (FTC) systems are needed to be designed and implemented for wind turbines in order to avoid unexpected shut downs and reduce maintenance costs. Therefore, FTC schemes could keep the turbines running from the time a fault is detected to the next planned service. In this thesis, we just scratched the surface. An advanced control system like SMC-based enhanced exponential reaching law (EERL) with Geometric approach can be considered as part of the FTC control design.

REFERENCES

Aubert, B., Regnier, J., Caux, S. & Alejo, D. (2015). Kalman-Filter-Based Indicator for Online Interturn Short Circuits Detection in Permanent-Magnet Synchronous Generators. *IEEE Transactions on Industrial Electronics*, 62(3), 1921–1930.

Beddek, K., Merabet, A., Kesraoui, M., Tanvir, A. A. & Beguenane, R. (2017). Signal-Based Sensor Fault Detection and Isolation for PMSG in Wind Energy Conversion Systems. *IEEE Transactions on Instrumentation and Measurement*, 66(9), 2403-2412.

Blaabjerg, F. & Ma, K. (2013). Future on Power Electronics for Wind Turbine Systems. *IEEE Journal of Emerging and Selected Topics in Power Electronics*, 1(3), 139-152.

Blaabjerg, F., Liserre, M. & Ma, K. (2012). Power Electronics Converters for Wind Turbine Systems. *IEEE Transactions on Industry Applications*, 48(2), 708-719.

CANWEA. (2020). Wind Turbine Installed Capacity. Consulted at https://canwea.ca/wind-energy/installed-capacity/.

Chaib, S., Boutat, D., Benali, A. & Kratz, F. (2009). Failure detection and reconstruction in switched nonlinear systems. *Nonlinear Analysis: Hybrid Systems*, 3(3), 225–238.

Cintron-Rivera, J. G., Foster, S. N. & Strangas, E. G. (2015). Mitigation of Turn-to-Turn Faults in Fault Tolerant Permanent Magnet Synchronous Motors. *IEEE Transactions on Energy Conversion*, 30(2), 465–475.

Da, Y., Shi, X. & Krishnamurthy, M. (2013). A New Approach to Fault Diagnostics for Permanent Magnet Synchronous Machines Using Electromagnetic Signature Analysis. *IEEE Transactions on Power Electronics*, 28(8), 4104–4112.

Delfino, F., Pampararo, F., Procopio, R. & Rossi, M. (2012). A Feedback Linearization Control Scheme for the Integration of Wind Energy Conversion Systems Into Distribution Grids. *IEEE Systems Journal*, 6(1), 85-93.

Ebrahimi, B., Faiz, J. & Roshtkhari, M. (2009). Static-, Dynamic-, and Mixed-Eccentricity Fault Diagnoses in Permanent-Magnet Synchronous Motors. *IEEE Transactions on Industrial Electronics*, 56(11), 4727–4739.

Fallaha, C. J., Saad, M., Kanaan, H. Y. & Al-Haddad, K. (2011). Sliding-Mode Robot Control With Exponential Reaching Law. *IEEE Transactions on Industrial Electronics*, 58(2), 600–610.

Gao, W. & Hung, J. (1993). Variable structure control of nonlinear systems: a new approach. *IEEE Transactions on Industrial Electronics*, 40(1), 45–55.

Ghodbane, A., Saad, M., Hobeika, C., Boland, J. & Thibeault, C. (2016). Design of a tolerant flight control system in response to multiple actuator control signal faults induced by cosmic rays. *IEEE Transactions on Aerospace and Electronic Systems*, 52(2), 681–697.

Hao, X., Yang, X., Liu, T., Huang, L. & Chen, W. (2013). A sliding-mode controller with multiresonant sliding surface for single-phase grid-connected VSI with an LCL filter. *IEEE Transactions on Power Electronics*, 28(5), 2259–2268.

Haq, I. U., Khan, Q., Khan, I., Akmeliawati, R., Nisar, K. S. & Khan, I. (2020). Maximum Power Extraction Strategy for Variable Speed Wind Turbine System via Neuro-Adaptive Generalized Global Sliding Mode Controller. *IEEE Access*, 8, 128536-128547.

Heier, S. (2014). *Grid Integration of Wind Energy*. John Wiley & Sons, Ltd.

IEA. (2020). Global Energy Review 2020. Consulted at https://www.iea.org/reports/global-energy-review-2020/renewables.

IRENA. (2019). FUTURE OF WIND: Deployment, investment,technology, grid integration andsocio-economic aspects. Consulted at https://www.irena.org/-/media/Files/IRENA/Agency/Publication/2019/Oct/IRENA_Future_of_wind_2019.pdf.

Isermann, R. (2006). *Fault-Diagnosis Systems*. Springer Berlin Heidelberg.

Islam, M., Mekhilef, S. & Saidur, R. (2013). Progress and recent trends of wind energy technology. *Renewable and Sustainable Energy Reviews*, 21, 456 - 468.

Jeong, I., Hyon, B. J. & Nam, K. (2013). Dynamic Modeling and Control for SPMSMs With Internal Turn Short Fault. *IEEE Transactions on Power Electronics*, 28(7), 3495–3508.

Kim, K., Jeung, Y., Lee, D. & Kim, H. (2012). LVRT Scheme of PMSG Wind Power Systems Based on Feedback Linearization. *IEEE Transactions on Power Electronics*, 27(5),

2376-2384.

Kim, S.-K., Song, H. & Lee, J.-H. (2015). Adaptive Disturbance Observer-Based Parameter-Independent Speed Control of an Uncertain Permanent Magnet Synchronous Machine for Wind Power Generation Applications. *Energies*, 8(5), 4496–4512.

Krause, P., Wasynczuk, O., Sudhoff, S. & Pekarek, S. (Eds.). (2013). *Analysis of Electric Machinery and Drive Systems*. John Wiley & Sons, Inc.

Kuschke, M. & Strunz, K. (2014). Energy-Efficient Dynamic Drive Control for Wind Power Conversion With PMSG: Modeling and Application of Transfer Function Analysis. *IEEE Journal of Emerging and Selected Topics in Power Electronics*, 2(1), 35-46.

Li, S., Haskew, T. A., Swatloski, R. P. & Gathings, W. (2012). Optimal and Direct-Current Vector Control of Direct-Driven PMSG Wind Turbines. *IEEE Transactions on Power Electronics*, 27(5), 2325-2337.

Lu, Q., of Manchester, U., University of Manchester. School of Mechanical, A. & Engineering, C. (2011). *Fault Diagnosis and Fault Tolerant Control of DFIG Based Wind Turbine System*. (Ph.D. thesis).

Massoumnia, M.-A. (1986). A geometric approach to the synthesis of failure detection filters. *IEEE Transactions on Automatic Control*, 31(9), 839–846.

Muyeen, S. M. & Al-Durra, A. (2013). Modeling and Control Strategies of Fuzzy Logic Controlled Inverter System for Grid Interconnected Variable Speed Wind Generator. *IEEE Systems Journal*, 7(4), 817-824.

Muyeen, S., Tamura, J. & Murata, T. (2009). *Stability Augmentation of a Grid-connected Wind Farm*. London, UK: Springer.

NRCAN. (2020). Renewable energy facts. Consulted at https://www.nrcan.gc.ca/science-data/data-analysis/energy-data-analysis/renewable-energy-facts/20069#L6.

Nyanteh, Y., Edrington, C., Srivastava, S. & Cartes, D. (2013). Application of Artificial Intelligence to Real-Time Fault Detection in Permanent-Magnet Synchronous Machines. *IEEE Transactions on Industry Applications*, 49(3), 1205–1214.

Orlando, N. A., Liserre, M., Mastromauro, R. A. & Dell'Aquila, A. (2013). A Survey of Control Issues in PMSG-Based Small Wind-Turbine Systems. *IEEE Transactions on Industrial Informatics*, 9(3), 1211–1221.

Persis, C. D. & Isidori, A. (2001). A geometric approach to nonlinear fault detection and isolation. *IEEE Transactions on Automatic Control*, 45(6), 853–865.

Polinder, H., van der Pijl, F. F. A., de Vilder, G. . & Tavner, P. J. (2006). Comparison of direct-drive and geared generator concepts for wind turbines. *IEEE Transactions on Energy Conversion*, 21(3), 725-733.

Qiu, Z., Zhou, K. & Li, Y. (2011, jul). Modeling and control of diode rectifier fed PMSG based wind turbine. *2011 4th International Conference on Electric Utility Deregulation and Restructuring and Power Technologies (DRPT).*

Rajaei, A., Mohamadian, M. & Yazdian Varjani, A. (2013). Vienna-Rectifier-Based Direct Torque Control of PMSG for Wind Energy Application. *IEEE Transactions on Industrial Electronics*, 60(7), 2919-2929.

Ribrant, J. & Bertling, L. M. (2007). Survey of Failures in Wind Power Systems With Focus on Swedish Wind Power Plants During 1997–2005. *IEEE Transactions on Energy Conversion*, 22(1), 167–173.

Rigatos, G., Siano, P. & Zervos, N. (2014). Sensorless Control of Distributed Power Generators With the Derivative-Free Nonlinear Kalman Filter. *IEEE Transactions on Industrial Electronics*, 61(11), 6369-6382.

Sarikhani, A. & Mohammed, O. A. (2013). Inter-Turn Fault Detection in PM Synchronous Machines by Physics-Based Back Electromotive Force Estimation. *IEEE Transactions on Industrial Electronics*, 60(8), 3472–3484.

Sarsembayev, B., Suleimenov, K., Mirzagalikova, B. & Do, T. D. (2020). SDRE-Based Integral Sliding Mode Control for Wind Energy Conversion Systems. *IEEE Access*, 8, 51100-51113.

Sebaaly, F., Vahedi, H., Kanaan, H. Y., Moubayed, N. & Al-Haddad, K. (2014, nov). Sliding-mode current control design for a grid-connected three-level NPC inverter. *International Conference on Renewable Energies for Developing Countries 2014*.

Sharifzadeh, M., Vahedi, H., Portillo, R., Khenar, M., Sheikholeslami, A., Franquelo, L. G. & Al-Haddad, K. (2016). Hybrid SHM-SHE Pulse-Amplitude Modulation for High-Power Four-Leg Inverter. *IEEE Transactions on Industrial Electronics*, 63(11), 7234-7242.

Shtessel, Y., Edwards, C., Fridman, L. & Levant, A. (2014). *Sliding Mode Control and Observation*. Springer New York.

Slootweg, J., de Haan, S., Polinder, H. & Kling, W. (2003). General model for representing variable speed wind turbines in power system dynamics simulations. *IEEE Transactions on Power Systems*, 18(1), 144–151.

Slotine, J. & Li, W. (1991). *Applied Nonlinear Control*. New Jersey, USA: Prentice Hall.

Tan, Y., Zhang, H. & Zhou, Y. (2020). Fault Detection Method for Permanent Magnet Synchronous Generator Wind Energy Converters Using Correlation Features Among Three-phase Currents. *Journal of Modern Power Systems and Clean Energy*, 8(1), 168-178.

Tavner, P. (2008). Review of condition monitoring of rotating electrical machines. *IET Electric Power Applications*, 2(4), 215.

Trilla, L., Bianchi, F. D. & Gomis-Bellmunt, O. (2014). Linear parameter-varying control of permanent magnet synchronous generators for wind power systems. *IET Power Electronics*, 7(3), 692-704.

Vahedi, H. & Al-Haddad, K. (2016). Real-Time Implementation of a Seven-Level Packed U-Cell Inverter with a Low-Switching-Frequency Voltage Regulator. *IEEE Transactions on Power Electronics*, 31(8), 5967-5973.

Vahedi, H., Labbé, P. & Al-Haddad, K. (2016). Sensor-Less Five-Level Packed U-Cell (PUC5) Inverter Operating in Stand-Alone and Grid-Connected Modes. *IEEE Transactions on Industrial Informatics*, 12(1), 361-370.

Valenciaga, F. & Puleston, P. (2008). High-Order Sliding Control for a Wind Energy Conversion System Based on a Permanent Magnet Synchronous Generator. *IEEE Transactions on Energy Conversion*, 23(3), 860–867.

Vaseghi, B., Takorabet, N. & Meibody-Tabar, F. (2009). Fault Analysis and Parameter Identification of Permanent-Magnet Motors by the Finite-Element Method. *IEEE Transactions*

on Magnetics, 45(9), 3290–3295.

Vaseghi, B., Takorabet, N., Nahid-Mobarakeh, B. & Meibody-Tabar, F. (2011). Modelling and study of PM machines with inter-turn fault dynamic model–FEM model. *Electric Power Systems Research*, 81(8), 1715–1722.

Wu, B., Lang, Y., Zargari, N. & Kouro, S. (2011). *Power conversion and control of wind energy systems*. Hoboken, New Jersey: Wiley.

Xia, C., Wang, Z., Shi, T. & Song, Z. (2013). A Novel Cascaded Boost Chopper for the Wind Energy Conversion System Based on the Permanent Magnet Synchronous Generator. *IEEE Transactions on Energy Conversion*, 28(3), 512–522.

Xia, Y., Fletcher, J., Finney, S., Ahmed, K. & Williams, B. (2011). Torque ripple analysis and reduction for wind energy conversion systems using uncontrolled rectifier and boost converter. *IET Renewable Power Generation*, 5(5), 377.

Xu, D., Blaabjerg, F., Chen, W. & Zhu, N. (2018). *Basics of Wind Power Generation System*.

Yaramasu, V. & Wu, B. (2014). Predictive Control of a Three-Level Boost Converter and an NPC Inverter for High-Power PMSG-Based Medium Voltage Wind Energy Conversion Systems. *IEEE Transactions on Power Electronics*, 29(10), 5308–5322.

Yaramasu, V., Wu, B., Alepuz, S. & Kouro, S. (2014). Predictive Control for Low-Voltage Ride-Through Enhancement of Three-Level-Boost and NPC-Converter-Based PMSG Wind Turbine. *IEEE Transactions on Industrial Electronics*, 61(12), 6832–6843.

Yuan, X., Wang, F., Boroyevich, D., Li, Y. & Burgos, R. (2009). DC-link Voltage Control of a Full Power Converter for Wind Generator Operating in Weak-Grid Systems. *IEEE Transactions on Power Electronics*, 24(9), 2178-2192.

Zafarani, M., Bostanci, E., Qi, Y., Goktas, T. & Akin, B. (2018). Interturn Short-Circuit Faults in Permanent Magnet Synchronous Machines: An Extended Review and Comprehensive Analysis. *IEEE Journal of Emerging and Selected Topics in Power Electronics*, 6(4), 2173–2191.

Zhang, W., Gadsden, S. A. & Habibi, S. R. (2013). Nonlinear estimation of stator winding resistance in a brushless DC motor. *2013 American Control Conference*, pp. 4699-4704.

Zhong, Q.-C., Ma, Z., Ming, W.-L. & Konstantopoulos, G. C. (2015). Grid-friendly wind power systems based on the synchronverter technology. *Energy Conversion and Management*, 89, 719 - 726.